PHYSICAL REVIEW D **82,** 113006 (2010)

Probing dark matter models with neutrinos from the Galactic center

Arif Emre Erkoca,[1] Mary Hall Reno,[2] and Ina Sarcevic[1,3]
[1]*Department of Physics, University of Arizona, Tucson, Arizona 85721, USA*
[2]*Department of Physics and Astronomy, University of Iowa, Iowa City, Iowa 52242, USA*
[3]*Department of Astronomy and Steward Observatory, University of Arizona, Tucson, Arizona 85721, USA*
(Received 14 September 2010; published 6 December 2010)

We calculate the contained and upward muon and shower fluxes due to neutrinos produced via dark matter annihilation or decay in the Galactic center. We consider dark matter models in which the dark matter particle is a gravitino, a Kaluza-Klein particle and a particle in leptophilic models. The Navarro-Frenk-White profile for the dark matter density distribution in the Galaxy is used. We incorporate neutrino oscillations by assuming maximal mixing and parametrize our results for muon and shower distributions. The muon and shower event rates and the minimum observation times in order to reach 2σ detection significance are evaluated. We illustrate how observation times vary with the cone half angle chosen about the Galactic center, with the result that the optimum angles are about 10° and 50° for the muon events and shower events, respectively. We find that for the annihilating dark matter models such as the leptophilic and Kaluza-Klein models, upward and contained muon as well as showers are promising signals for dark matter detection in just a few years of observation, whereas for decaying dark matter models, the same observation times can only be reached with showers. We also illustrate for each model the parameter space probed with the 2σ signal detection in five years. We discuss how the shape of the parameter space probed change with significance and the observation time.

DOI: 10.1103/PhysRevD.82.113006 PACS numbers: 95.35.+d, 14.60.Lm, 95.55.Vj, 95.85.Ry

I. INTRODUCTION

The identity of dark matter (DM), which constitutes 23% of the total density of the Universe [1], has been one of the most important open questions in astrophysics for more than seven decades [2]. Concerted theoretical and observational efforts are being made to detect the DM through photonic and leptonic signals [3–19]. Extensions of the standard model of particle physics have been proposed to account for the observed anomalies in the PAMELA positron and FERMI electron plus positron data [4,5,7,9,10,16–18]. These models also predict neutrino production via DM annihilation or decay [20–27].

Neutrino signals are complementary to photon or charged lepton signals from the Galactic center, or more generally from the Galactic halo. Neutrinos with energies of the order of the DM mass, $E_\nu < m_\chi$ for $m_\chi \leq 10$ TeV, propagate without being absorbed or deflected in transit toward the Earth. Neutrino telescopes have the capabilities to probe higher energies than the satellite based telescopes [28,29]. The approaches to DM searches, including the optimal angular coverage of the Galactic center or halo, are different depending on the details of the DM model and the location of the detector relative to the Galactic center. The strategies for uncovering neutrino signals of DM decay or annihilation in the Galactic halo seen in underground or underwater detectors are the subject of this paper.

We calculate the neutrino induced contained and upward muon flux, hadronic shower flux and the muon and shower event rates for different DM models which are considered to explain data excesses in other indirect DM searches. In this paper, we study the annihilation of the lightest Kaluza-Klein particle [14,30], leptophilic DM particle annihilation [7,16], two-body and three-body decay channels of gravitino, as well as the decay of the leptophilic DM [10,15–17,23,24]. We show that for each model, the shape of the muon and shower fluxes differs significantly from the shape of the neutrino fluxes at production due to the smearing produced by neutrino interactions and muon propagation as discussed in Refs. [31,32]. We also calculate the detection significances of the DM signals at the IceCube/DeepCore [28] detector and compare the different DM models in terms of the energy spectra and the total counts of the muon and shower events. We show the parameter space of different DM models that is being probed when we require 2σ muon or shower signal within five years of observation.

II. MODELS FOR DARK MATTER

The ingredients for theoretical predictions of particle fluxes from DM annihilation or decay include a model for the DM distribution, a particle physics model for the DM particle couplings to standard model particles, and standard model physics processes for the resulting produced particles. For the DM distribution in the galaxy, we use the Navarro-Frenk-White (NFW) [33] profile as a typical realistic DM density profile. The expressions for the neutrino fluxes and its dependence on the DM profile are presented in Appendix A. In case of DM decay (annihilation), the neutrino spectrum has linear (quadratic) dependence on the DM density.

The particle physics models on which we focus in this study consist of the leptophilic, Kaluza-Klein and gravitino dark matters. Either thermal averaged annihilation cross section times velocity $\langle\sigma v\rangle$ or a decay time τ specific to the model is required. Characteristically for annihilation, the required $\langle\sigma v\rangle$ is larger [16,19,22,25,26] than the value required for a thermal relic abundance [34]: $\langle\sigma v\rangle_0 = 3 \times 10^{-26}$ cm^3 s^{-1}. Following the current convention, we write

$$\langle\sigma v\rangle = B\langle\sigma v\rangle_0, \tag{1}$$

with a boost factor B. There are theoretical evaluations of the boost factor [35], however, we treat the boost factor as a phenomenological parameter in this paper. To explain the lepton excesses, some models have constraints on the boost factor as a function of DM mass [16].

In leptophilic DM models [7,16] explaining the PAMELA positron excess, the DM annihilation or decay must proceed dominantly to leptons in order to avoid the overproduction of antiprotons. Moreover, according to the FERMI data, the direct production of electrons must be suppressed with respect to the production of electrons (and positrons) as secondaries. It was shown [16] that the leptophilic DM with mass (m_χ) in the range between 150 GeV and a few TeV, which annihilates or decays into τ's or μ's, can fit the PAMELA [4] and Fermi [5] data as well as the HESS high energy photon data [6]. The best fit parameters for the boost factor (B) and the decay time (τ) which determine the overall normalizations, for the specific case involving muons from annihilation ($\chi\chi \to \mu^+\mu^-$) or decay ($\chi \to \mu^+\mu^-$), respectively, are given by [16]

$$\begin{aligned} B &= 431 m_\chi - 38.9 \\ \tau &= \left(2.29 + \frac{1.182}{m_\chi}\right) \times 10^{26}\ \text{sec} = B_\tau \times 10^{26}\ \text{sec} \end{aligned} \tag{2}$$

for m_χ in TeV. The annihilation channel into tau pairs is less favored by the data [16].

Some Kaluza-Klein models can provide a DM candidate which gives the correct relic density [30]. To account for the HESS results [6], the lightest Kaluza-Klein particle (LKP) would have a mass of the order of a TeV [14]. The LKP is also assumed to be neutral and nonbaryonic. In this model, the particle couplings are fixed such that LKP pairs annihilate into quark pairs (35%), charged lepton pairs (59%), neutrinos (4%), gauge bosons (1.5%) and Higgs bosons (0.5%) [14,30].

The first DM candidate proposed in the context of supersymmetry is the gravitino ($\psi_{3/2}$) which would be the lightest supersymmetric particle (LSP). The gravitino is the superpartner of the graviton. With the existence of small R-parity breaking to allow the LSP to decay, the gravitino decays into standard model particles. The decay rate of the gravitino in this scenario is so small that it can have a sufficiently long lifetime for the correct DM relic density today.

In order to account for the observed anomalous positron excess in the PAMELA data and positron plus electron excess in the FERMI data, the lifetime of the gravitino DM is constrained to be of the order of $\sim 10^{26}$ seconds and its mass to be in the range between few 100 GeV and few TeV [17]. To explain the data, the three-body gravitino decay mode ($\psi_{3/2} \to l^+ l^- \nu$) was considered [17]. We use the parameters of this model to explore neutrino signals from gravitino decay. For illustration, in addition to three-body decay, we also consider the two-body gravitino decay modes ($\psi_{3/2} \to (W^{\mp} l^{\pm}, Z\nu, \gamma\nu)$) assuming the same lifetime and mass as for the three-body decay, and with the branching fractions given in Table I.

Selected DM model parameters are shown in Table II. For each of the DM models considered, the decay distribution of the produced particles to neutrinos in the case of DM annihilation, or the gravitino decay distribution to neutrinos, enters into the calculation of the neutrino fluxes that arrive at Earth. For annihilation directly to neutrinos, the energy distribution of each neutrino is a delta function in energy, with the energy equal to the DM mass. This case has been well studied in the literature [21,31,32,36]. Here, we look at the secondary neutrinos. Figure 1 shows neutrino spectra, plotted in terms of $x \equiv E_\nu/E_{\nu,\max}$, where $E_{\nu,\max} = m_\chi$ for annihilating DM and $E_{\nu,\max} = m_\chi/2$ for decaying DM models. The curves in the figure are normalized to count the number of neutrinos, and in the case of the $Z\nu$ final state, the fraction of Z decays to neutrinos. The muon neutrino spectra in the figure should be multiplied by the branching fraction for a specific decay channel in a

TABLE I. Branching fractions for the two-body gravitino decay into different R-parity violating channels for different masses [15].

$m_{\psi_{3/2}}$ (GeV)	$B_F(\psi_{3/2} \to \gamma\nu)$	$B_F(\psi_{3/2} \to Wl)$	$B_F(\psi_{3/2} \to Z\nu)$
10	1	0	0
85	0.66	0.34	0
100	0.16	0.76	0.08
150	0.05	0.71	0.24
200	0.03	0.69	0.28
400	0.03	0.68	0.29

TABLE II. Model parameters characterizing fits to explain FERMI and PAMELA anomalies used as examples in this paper.

Particle/mode	mass	B_τ or B
$\psi_{3/2} \to l^+ l^- \nu$	400 GeV	$B_\tau = 2.3$
$\psi_{3/2} \to (Wl, Z\nu, \gamma\nu)$	400 GeV	$B_\tau = 2.3$
$\chi \to \mu^+\mu^-$	2 TeV	$B_\tau = 2.9$
$B^{(1)}B^{(1)} \to (q\bar{q}, l^+l^-, W^+W^-, ZZ, \nu\bar{\nu})$	800 GeV	$B = 200$
$\chi\chi \to \mu^+\mu^-$	1 TeV	$B = 400$

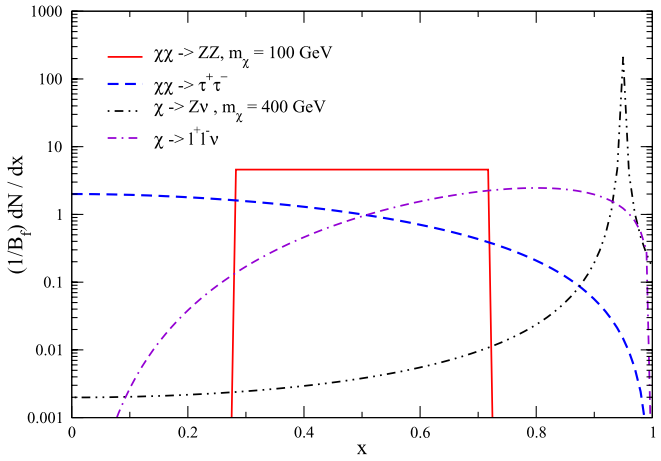

FIG. 1 (color online). Muon neutrino (ν_μ) spectra in terms of $x = E_\nu/E_{\nu,\max}$ from the three-body decay of gravitino (dot-dash-dashed line), from the decay of τ (dashed line), Z boson (solid line) and from one of the two-body decay channels of gravitino ($\psi \to Z\nu$) for which Breit-Wigner distribution is used. The distributions should be multiplied by the branching fractions, and oscillations should be taken into account for the flux of neutrinos at Earth.

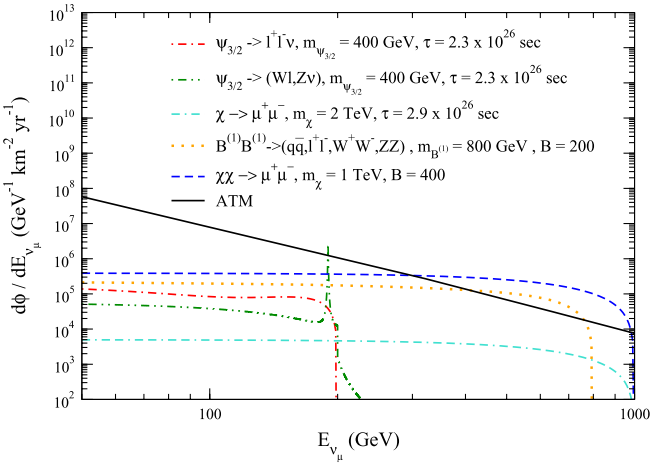

FIG. 2 (color online). Muon neutrino (ν_μ) fluxes from the annihilation of the Kaluza-Klein (dotted line), leptophilic (dashed line), and the decay of leptophilic (dash-dot-dashed line), three-body decay (dot-dashed line) and two-body decay (dot-dot-dashed line) of gravitino DM particles. Neutrino oscillations have been taken into account. The angle-averaged atmospheric muon neutrino flux at the surface of the Earth is also presented (solid line). The corresponding values of the parameters for each model are shown as well.

given model. Analytic expressions for the neutrino spectra are given in Appendix B.

III. NEUTRINO FLUX

The neutrino flux at Earth can be evaluated using the neutrino flux expressions given by Eqs. (A1) and (A2) in Appendix A and the neutrino spectra given in Appendix B with taking the neutrino oscillation effects into account. In Fig. 2, we show the muon neutrino flux at Earth for three decay channels and two annihilation channels.

In some DM models all three flavors of neutrinos can be generated by DM annihilation or decay, implying the flavor ratio $\nu_e{:}\nu_\mu{:}\nu_\tau$ at the production site to be 1:1:1. This ratio remains unchanged with oscillation. This is the case for the gravitino decay and Kaluza-Klein DM annihilation. However, in case of the leptophilic DM model, in which $\chi \to \mu^+\mu^-$, the initial neutrino flavor ratio is 1:1:0 which becomes 1:0.5:0.5 as neutrinos travel astrophysical distances. We take this oscillation effect into account when we evaluate muon neutrino fluxes presented in Fig. 2 and when we evaluate muon event rates below.

Figure 2 shows that with the exception of the gravitino decays, the distributions of neutrinos have very weak energy dependence. The two-body gravitino decay gives a spiked feature at the kinematic limit in neutrino energy. The relative normalizations of the DM curves come from different DM lifetimes or boost factors.

Also shown in Fig. 2 is the angle-averaged atmospheric muon neutrino flux at the surface of the Earth. It is characterized by an approximate formula [31,37], (in units of $\mathrm{GeV}^{-1}\,\mathrm{km}^{-2}\,\mathrm{yr}^{-1}\,\mathrm{sr}^{-1}$)

$$\left(\frac{d\phi_\nu}{dE_\nu d\Omega}\right)_{\mathrm{ATM,avg}} = N_0 E_\nu^{-\gamma-1}\left(\frac{a}{bE_\nu}\ln(1+bE_\nu) + \frac{c}{eE_\nu}\ln(1+eE_\nu)\right), \tag{3}$$

where the parameters in the formula are listed in Table III. These same parameters appear in the angle-dependent atmospheric neutrino flux for zenith angle θ,

$$\frac{d\phi_\nu}{dE_\nu d\Omega} = N_0 E_\nu^{-\gamma-1} \times \left(\frac{a}{1+bE_\nu\cos\theta} + \frac{c}{1+eE_\nu\cos\theta}\right). \tag{4}$$

This formula does not account for the prompt neutrino flux [38], however, for the energy range of interest, the prompt atmospheric neutrino flux is negligible.

The angle-averaged atmospheric neutrino flux is a good approximation. In Fig. 3, we show the angle-averaged flux from Eq. (4) and the flux from Eq. (5) with $\theta = 60°$ and the

TABLE III. Parameters for the atmospheric ν_μ and $\bar{\nu}_\mu$ fluxes given by Eqs. (3) and (4), in units of $\mathrm{GeV}^{-1}\,\mathrm{km}^{-2}\,\mathrm{yr}^{-1}\,\mathrm{sr}^{-1}$ [37].

γ	1.74
a	0.018
b	0.024 GeV^{-1}
c	0.0069
e	0.00139 GeV^{-1}
N_0	1.95×10^{17} for ν
	1.35×10^{17} for $\bar{\nu}$

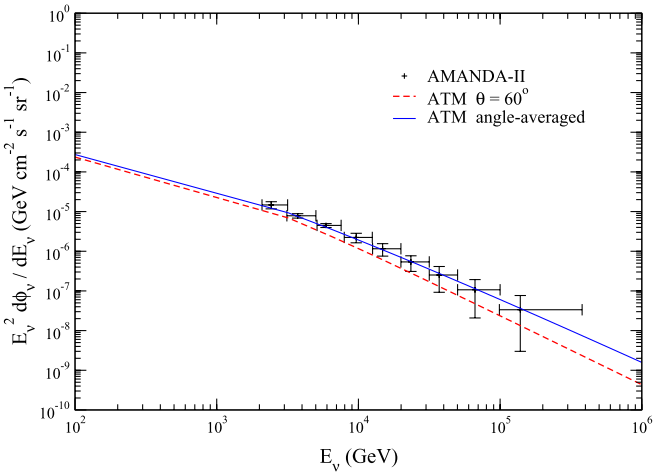

FIG. 3 (color online). Angle-averaged atmospheric muon neutrino ($\nu_\mu + \bar{\nu}_\mu$) flux (solid line) and the atmospheric flux for fixed $\theta = 60°$ (dashed line) compared with the angle-averaged ($\nu_\mu + \bar{\nu}_\mu$) flux from AMANDA-II muon neutrino flux measurements [39].

integrated flux measured by the AMANDA-II detector from Ref. [39]. The angle-averaged flux is a bit larger than the flux at 60°, so at least for θ less than 60°, using the angle-averaged atmospheric flux gives a small overestimate of the atmospheric background.

IV. NEUTRINO SIGNALS

For each DM candidate and model, there are several signals to pursue in underground detectors. One possibility is to measure or constrain the rate of muons produced by muon neutrinos, over and above the expected atmospheric background rate. High energy muons point essentially in the same direction as the incident neutrino, and the angular resolution of high energy muon tracks is quite good. With good enough energy and angular resolution, and a large enough target volume, one looks for neutrinos coming directly from DM annihilation in the Galactic center, however, the target volume may be a limitation for constraining model parameters including the boost factor. A comparison of the upward-going muon rate, where the target volume is enhanced by the muon range at high energies, and the contained rate of muon production by neutrinos in the detector, is a useful exercise.

For the IceCube/DeepCore detector, the Galactic center is above the horizon, so the upward muon rate of DM produced neutrinos is from the Galactic halo in a direction pointing away from the Galactic center. We consider this possibility as well.

Showers, either electromagnetic or hadronic, are produced by neutrinos. We look at the optimization for these as well as a function of cone half angle, but we note that the current capabilities for shower angular resolution are somewhat limited, on the order of 50° [40,41].

A. Muons

The neutrinos coming from the Galactic center and Galactic halo can produce muons through charged current interactions in the detector (contained muons). The flux is given by

$$\frac{d\phi_\mu}{dE_\mu} = \int_{E_\mu}^{E_{\max}} dE_\nu \left(\frac{d\phi_\nu}{dE_\nu}\right) \frac{N_A \rho}{2} \times \left(\frac{d\sigma_\nu^p(E_\nu, E_\mu)}{dE_\mu} + (p \to n)\right) + (\nu \to \bar{\nu}), \quad (5)$$

where $N_A = 6.022 \times 10^{23}$ is Avogadro's number, ρ is the density of the medium, $E_{\max} = m_\chi$ for annihilation and $E_{\max} = m_\chi/2$ for decay. The differential cross sections $d\sigma_\nu^{p,n}/dE_\mu$ are the weak scattering charged-current cross sections for neutrino and antineutrino scattering with protons and neutrons [42].

We evaluate the muon flux from neutrino charged-current interactions in the detector, when neutrinos are produced in DM annihilation or DM decay. In Fig. 4 we show muon fluxes for the case when the DM particle is a gravitino, a Kaluza-Klein particle and for a leptophilic model in which DM annihilation or decay produces $\mu^+\mu^-$, for the model parameters listed in Table II. We take the cone half angle around the Galactic center to be $\theta_{\max} = 1°$.

In case of the gravitino DM decay and for Kaluza-Klein DM annihilation, there are discontinuities in the slopes at the highest muon energies coming from the superposition of the direct neutrino production (dot-dot-dashed line for DM decay and dotted line for the Kaluza-Klein annihilation). The direct neutrino production, $\chi\chi \to \nu\bar{\nu}$, is the "golden channel" for DM detection because in this case

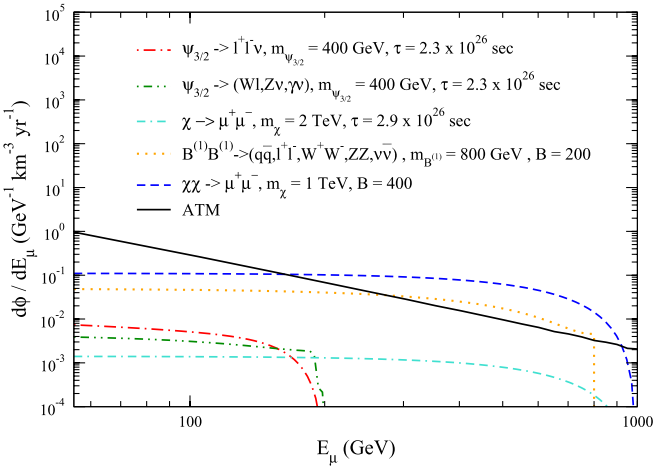

FIG. 4 (color online). Muon flux for the contained events for gravitino decay (dot-dashed and dot-dot-dashed lines), Kaluza-Klein annihilation (dotted line), leptophilic model (dashed line for annihilation and dash-dash-dotted line for decay) compared with the atmospheric background (solid line), for the case when $\theta_{\max} = 1°$. Model parameters are given in Table II.

the muon flux is increasing with energy, and it peaks at $E_\mu = m_\chi$ [32].

As noted in Sec. II, the parameters used for DM masses, boost factors and lifetimes are characteristic of those that were shown to describe PAMELA, Fermi/LAT and HESS data [14,16,17]. Changing the value of the boost factor or the lifetime affects only the overall normalization of the muon flux. We find that for this choice of the parameters, DM signals in leptophilic model exceed the atmospheric background for $E_\mu > 175$ GeV, while for the Kaluza-Klein DM model the signal is above the background for $E_\mu > 275$ GeV. In both cases, the signal cuts off when $E_\mu = m_\chi$.

We consider the effect on the muon flux shape when we change the parameters, for example, for the leptophilic model. In Fig. 5 we show the contained muon flux from DM annihilation and decay in a leptophilic model for different values of the parameters B, τ and m_χ, which are constrained to satisfy Eq. (2) to describe the data [16]. The decays (lower thin lines) have lower fluxes than the annihilations (upper thick lines), even though the shapes are similar. For leptophilic models, one cannot enhance the signal rate by increasing B or decreasing τ with m_χ fixed if the Fermi and PAMELA data are explained by the model.

Contained muons, produced by neutrino interactions in the detector, make up one set of muon signals. Muons can also be produced in neutrino interaction in the rock below the detector. Muons produced with energy E^i_μ, interact with the medium and finally reach the detector with energy E_μ. The effective volume of the detector is enhanced by the muon range at high energies. We denote these events as upward muon events.

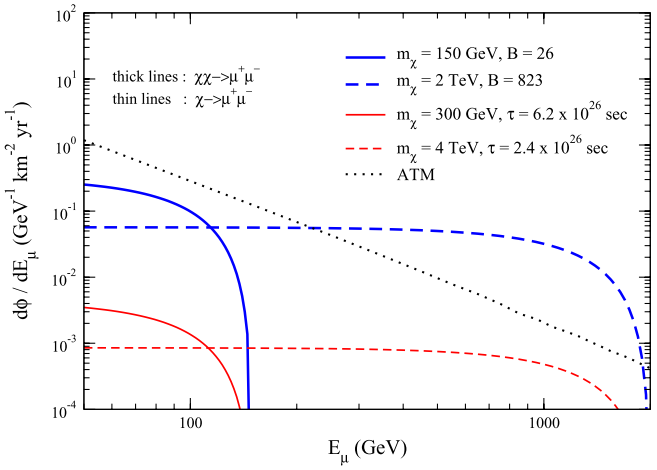

FIG. 5 (color online). Contained muon flux from the annihilation, $\chi\chi \to \mu^+\mu^-$ (thick lines), and the decay, $\chi \to \mu^+\mu^-$ (thin lines), processes. The relation between the boost factor and m_χ and between the lifetime and m_χ are given by Eq. (2). We take $\theta_{\max} = 1°$.

The muon range in the rock, $R_\mu(E^i_\mu, E_\mu)$, depends on the initial muon energy E^i_μ, the final energy E_μ and the parameters α and β which characterize muon energy loss. Numerically, $\alpha \simeq 2 \times 10^{-3}$ GeV cm^2/g accounts for the ionization energy loss and $\beta \simeq 3.0 \times 10^{-6}$ cm^2/g for the bremsstrahlung, pair production and photonuclear interactions. The range is then approximated by $R_\mu(E^i_\mu, E_\mu) = \ln[(E^i_\mu + \alpha/\beta)/(E_\mu + \alpha/\beta)]/\beta\rho$. For muon transit through the rock, the muon range is 1 km for $E^i_\mu \simeq 1$ TeV.

Taking into account the energy losses, the final muon flux at the position of the detector can be written as [31],

$$\frac{d\phi_\mu}{dE_\mu} = \int_0^{R_\mu(E^i_\mu, E_\mu)} e^{\beta\rho z} dz \times \int_{E^i_\mu}^{E_{\max}} dE_\nu \left(\frac{d\phi_\nu}{dE_\nu}\right) \times P_{\rm surv}(E^i_\mu, E_\mu) \times \frac{N_A \rho}{2}\left(\frac{d\sigma^p_\nu(E_\nu, E_\mu)}{dE_\mu} + (p \to n)\right) + (\nu \to \bar{\nu}), \quad (6)$$

where $P_{\rm surv}(E^i_\mu, E_\mu)$ is the survival probability for a muon with initial energy E^i_μ to reach final energy E_μ. A detailed derivation of Eq. (6) can be found in Ref. [31]. To first approximation, $P_{\rm surv} \simeq 1$ since at high energies, the muon has a long decay length. The muon energy at the production point is related to the muon energy a distance z from that point by

$$E^i_\mu(z) \simeq e^{\beta\rho z} E_\mu + (e^{\beta\rho z} - 1)\frac{\alpha}{\beta}. \quad (7)$$

We show in Fig. 6, the upward muon flux for a generic northern hemisphere detector, looking down through the Earth with a cone half angle of $\theta_{\max} = 1°$ around the Galactic center. The muon fluxes are smoothed relative to Fig. 4 as a consequence of the energy loss. For DM particles with masses of order 1 TeV, the upward muon flux

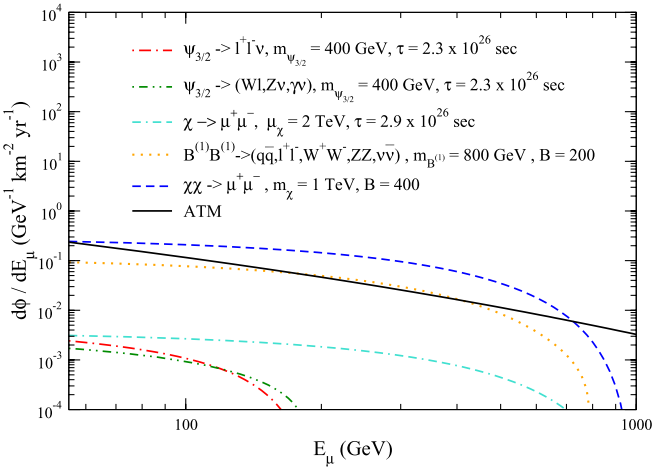

FIG. 6 (color online). Upward muon flux for the annihilating and decaying DM models from Table II. We take $\theta_{\max} = 1°$.

is larger at low energies than for the contained muons because the muon range is larger than 1 km, effectively enhancing the volume of the kilometer-size detector. When $m_\chi = 400$ GeV, the energies of the produced muons are such that the muon range is less than 1 km, which is the size of the detector for which the contained muon flux was calculated. If the depth of the detector is 500 m, the contained and upward muon fluxes for the DM mass of 400 GeV would be approximately equal at low energies, although the contained muon flux would have a little harder spectrum. This is direct consequence of muon range dependence on the DM mass. For example, muon with initial energy of 400 GeV (1 TeV) has a range of 500 m (1 km).

The contained muon event rate, $N_\mu^{ct}(m_\chi)$, is obtained by integrating muon flux folded with the effective volume of the detector, $V_{\rm eff}$, i.e.

$$N_\mu^{ct}(m_\chi) = \int_{E_\mu^{\rm th}}^{E_{\rm max}} \frac{d\phi_\mu^{ct}}{dE_\mu} V_{\rm eff}(E_\mu) dE_\mu \tag{8}$$

where $d\phi_\mu^{ct}/dE_\mu$ is given in Eq. (5) and $E_\mu^{\rm th}$ is the muon detector threshold, typically 10–100 GeV for deep ice or water detectors [28]. In our calculations, we choose $E_\mu^{\rm th} = 50$ GeV. We also consider an energy independent IceCube/DeepCore effective volume, $V_{\rm eff} = 0.04$ km^3, for the contained muon events [27,40].

Similarly, the upward muon event rate, is obtained by

$$N_\mu^{\rm up}(m_\chi) = \int_{E_\mu^{\rm th}}^{E_{\rm max}} \frac{d\phi_\mu^{\rm up}}{dE_\mu} A_{\rm eff}(E_\mu) dE_\mu \tag{9}$$

where $d\phi_\mu^{\rm up}/dE_\mu$ is given by Eq. (6), $A_{\rm eff}$ is the angle-averaged muon effective area for which we assume $A_{\rm eff} = 1$ km^2.

The event rates for contained and upward muons for a cone half angle of $\theta_{\rm max} = 1^\circ$ are shown in Table IV for the DM models shown in Figs. 4 and 6 and listed in Table II. We also obtain the number of years required for the rate of signal events s and background events b to satisfy the condition

$$\frac{s}{\sqrt{s+b}} \geq 2. \tag{10}$$

From Table IV we note that for the parameters that we considered, only the Kaluza-Klein DM and leptophilic annihilation models have a reasonable chance of detection for $\theta_{\rm max} = 1^\circ$.

The model parameters such as DM masses, annihilation cross sections and decay times that we consider are introduced to explain some indirect DM searches as explained in the previous section. However, it is also possible that the signals that have been observed [4–6] in these searches have no DM origin. Then, m_χ and B or τ can be varied independently. In terms of the neutrino signals, the dependence of the signals on the annihilation cross sections or on the decay times is trivial since these parameters affect only the overall normalization. The dependence on DM mass is not that straightforward.

In order to see the dependence of the signals on DM mass, we set the values of the boost factor and the decay times to those in Table II and calculate the event rates as a function of DM mass for each model. We present our results for the contained muon event rates in Fig. 7 and for the upward muons in Fig. 8. The solid line in each figure corresponds to the muon background due to the atmospheric neutrinos.

From Fig. 7 we note that the contained muon events rates for annihilating DM models decrease with m_χ. On the other hand the event rates for the decaying DM models increase slowly with m_χ, for $m_\chi < 1$ TeV and for $m_\chi > 1$ TeV, they become almost independent of m_χ. The m_χ dependence of the contained muon event rates is mainly due to the m_χ^{-2} (m_χ^{-1}) dependence in the neutrino flux for DM annihilation (DM decay) combined with the upper limit of integration dependence on m_χ. For DM masses in the range $E_\mu^{\rm th} < m_\chi < 400$ GeV, where $E_\mu^{\rm th} = 50$ GeV, the integration region is sensitive to the value of the DM mass, while for $m_\chi \gg E_\mu^{\rm th}$ there is only weak dependence on m_χ. These combined effects are responsible for the observed m_χ dependence of the contained muon event rates presented in Fig. 7.

TABLE IV. Event rates per year and the time required to reach 2σ detection significance for the upward and the contained muons (μ) for a cone half angle of $\theta_{\rm max} = 1^\circ$. Results for different DM models are obtained by taking $A_{\rm eff} = 1$ km^2 and $V_{\rm eff} = 0.04$ km^3 for the upward and contained muon events, respectively.

	$A_{\rm eff} = 1$ km^2		$V_{\rm eff} = 0.04$ km^3	
	$N_\mu^{\rm up}$	t (yr)	N_μ^{ct}	t (yr)
$\psi_{3/2} \to l + l - \nu$	0.12	7811	0.0224	1.8×10^4
$\psi_{3/2} \to (Wl, Z\nu, \gamma\nu)$	0.1	1.1×10^4	0.0156	3.8×10^4
$\chi \to \mu^+\mu^-$	0.6	317	0.027	1.2×10^4
$B^{(1)}B^{(1)} \to (q\bar{q}, l^+l^-, \nu\bar{\nu}, \ldots)$	16	0.7	0.72	23
$\chi\chi \to \mu^+\mu^-$	46	0.14	2.1	4
ATM	28		2.28	

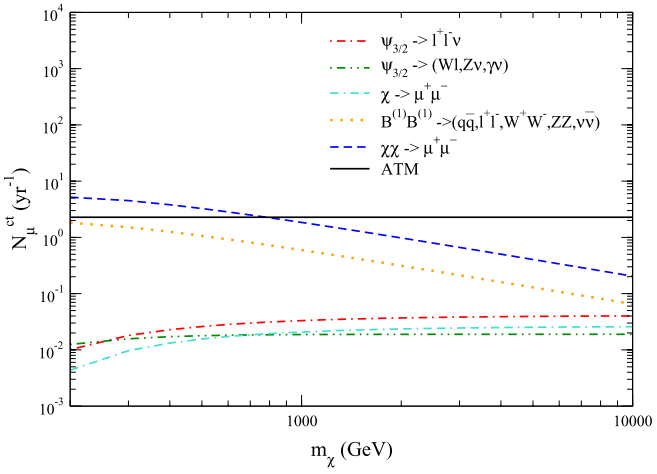

FIG. 7 (color online). Contained muon rates as a function of DM mass for the models presented in Table II. We take the muon detector threshold to be $E_\mu^{\rm th} = 50$ GeV and the cone half angle to be $\theta_{\rm max} = 1^\circ$.

The m_χ dependence of the upward muon rates is shown in Fig. 8. We find that the event rates for decaying DM models increase with m_χ while for annihilating DM models there is almost no m_χ dependence for a wide range of DM masses. In contrast to the contained muon rates, for upward muons there is additional m_χ that is present in the muon range. As we increase the value of DM mass, the effective volume which depends on the muon range in rock becomes larger.

The upward muon rates for a decaying DM particle have steeper increase with increasing DM mass than for contained muon rates, because of the energy dependent effective volume which increases with m_χ, when compared to the case for the contained muon events.

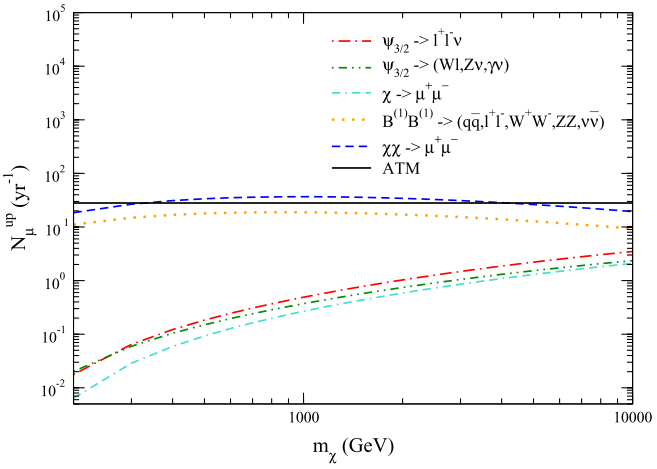

FIG. 8 (color online). Upward muon rates as a function of DM mass for the DM models presented in Table II. We take the muon detector threshold to be $E_\mu^{\rm th} = 50$ GeV and the cone half angle to be $\theta_{\rm max} = 1^\circ$.

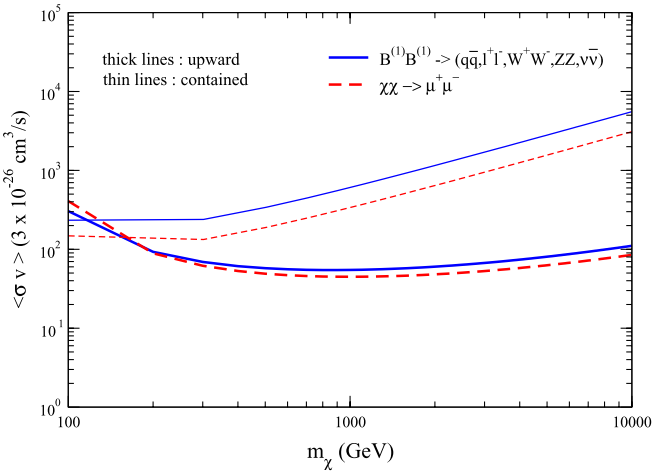

FIG. 9 (color online). Annihilation cross section versus DM mass for upward and for contained muon events to reach 2σ detection significance with five years of observation for the case of Kaluza-Klein (solid lines) and leptophilic (dashed lines) models. We take $\theta_{\rm max} = 1^\circ$ and $E_\mu^{\rm th} = 50$ GeV.

In Fig. 9, we present results for DM annihilation cross section required for a given DM mass in order to reach 2σ detection significance in five years of observation within $\theta_{\rm max} = 1^\circ$ for Kaluza-Klein (solid lines) and annihilating leptophilic (dashed lines) models. From Fig. 7 we note that the contained muon event rates decrease with m_χ for a fixed annihilation cross section (i.e. fixed boost factor). Therefore, in order to have the same detection significance for each DM mass, the DM annihilation cross section needs to increase with m_χ as shown in Fig. 9. However, for the upward muons, the event rates increase with m_χ for $m_\chi <$ 1 TeV and exhibit a slight decrease for higher DM masses for a fixed annihilation cross section. Thus, in order to have the same significance independent of the DM mass for the upward muon events the DM annihilation cross section has to decrease with m_χ for $m_\chi < 1$ TeV and increase for $m_\chi > 1$ TeV as seen in Fig. 9. If there is no signal detected at 2σ level in five years, the parameter space above each curve is excluded at that significance level. Our results also indicate that the upward muons are more promising than the contained muons in constraining the model parameters. Increasing the observation time would result in larger excluded parameter space.

Similar to the models for the annihilating DM, we evaluate the parameter space for the decaying DM models. In Fig. 10 we show the decay time as a function of the DM mass for $\theta_{\rm max} = 1^\circ$ that is needed in order to reach 2σ detection significance with a 5 yr observation period. For a wide range of DM masses, the contained muon event rates have weak dependence on m_χ, while the upward muon event rates show a steep increase with increasing m_χ as can be seen from Figs. 7 and 8. This implies that we need longer decay time for the upward muon events than for the

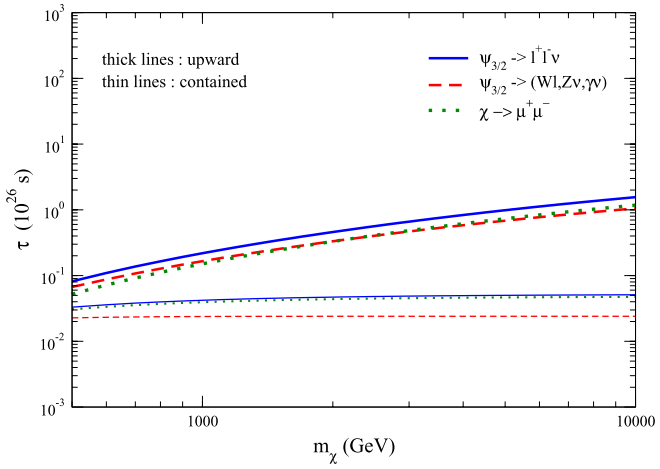

FIG. 10 (color online). Decay time versus DM mass for upward and for contained muon events to reach 2σ detection significance with five years of observation for the case of decaying DM models: gravitino three-body (solid lines), gravitino two-body (dashed lines) and leptophilic (dotted lines). We take $\theta_{\max} = 1^\circ$ and $E_\mu^{\rm th} = 50$ GeV.

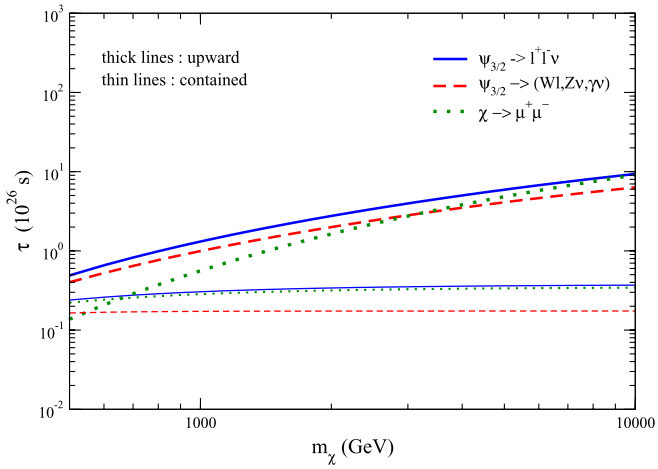

FIG. 11 (color online). Decay time versus DM mass for both upward and contained muon events to reach 2σ detection significance after five years of observation for the case of decaying DM models: gravitino three-body (solid lines), gravitino two-body (dashed lines) and leptophilic (dotted lines). We take $\theta_{\max} = 10^\circ$ and $E_\mu^{\rm th} = 50$ GeV.

contained muon events to reach the same detection significance for a 5 yr observation time while the decay time has almost no dependence on the DM mass for the contained muon events. The parameter space below each curve corresponds to the exclusion region at 2σ level after five years of no signal detection.

B. Optimal angles and muon signals

As noted earlier, the size of the cone (cone half angle value) that is too small can restrict the number of events too much. In Fig. 11, we present contour plots similar to those in Fig. 10 but for $\theta_{\max} = 10^\circ$. With increasing $\theta_{\max}$ from 1° to 10°, the J factor ($\langle J_1\rangle_\Omega \Delta\Omega$) entering into the neutrino flux increases, resulting in stronger restriction on the DM lifetime.

For more general use in discussing the dependence on cone half angles, the values of $\langle J_1\rangle_\Omega \Delta\Omega$ and $\langle J_2\rangle_\Omega \Delta\Omega$ given in Appendix A can be combined with the parametric forms for the muon fluxes given in Appendix C to calculate event rates for different cone half angles around the Galactic center. We note that the cone size dependence of the J factors is quite different for the case of DM annihilation than for decaying DM.

The difference between DM density contributions to DM annihilation and decay can also be seen in Fig. 20 in Appendix A, where we present $\langle J_n\rangle_\Omega \Delta\Omega$ factors for DM annihilation ($n = 2$) and DM decay ($n = 1$) evaluated for a cone wedge between $\theta_{\max} - 1^\circ$ and $\theta_{\max}$ around the Galactic center. We note that moving the wedge away from the Galactic center leads to a significant reduction of the signal from annihilating DM due to the dependence of $\langle J_2\rangle_\Omega \Delta\Omega$ on the square of the density (see Eq. (A3)). We find that the signal is reduced by a factor of 17 when the wedge is moved from 1° to 90° off the Galactic center. On the other hand, in a wedge between 50° and 90° around the Galactic center, the value of $\langle J_2\rangle_\Omega \Delta\Omega$ is about 5.6, a value close to what one obtains for a cone centered at the Galactic center with $\theta_{\max} = 5^\circ$.

In contrast, for a decaying DM, the signal from a wedge between $\theta_{\max} - 1^\circ$ and $\theta_{\max}$ around the Galactic center increases with $\theta_{\max}$ for $\theta_{\max} < 30^\circ$ and decreases slowly for higher $\theta_{\max}$. For example, $\langle J_1(1^\circ)\rangle_\Omega \Delta\Omega = 0.018$ whereas $\langle J_1(30^\circ) - J_1(29^\circ)\rangle_\Omega \Delta\Omega = 0.2$ which is only a factor of 2 higher than $\langle J_1(90^\circ) - J_1(89^\circ)\rangle_\Omega \Delta\Omega = 0.1$. This is a consequence of the dependence of the signal for a decaying DM particle on density which is one power less when compared to an annihilating DM particle. An increase in the size of the wedge (i.e., the volume of the source region) can result in an enhancement in the signal even if the chosen wedge is away from the Galactic center.

TABLE V. Shower event rates per year and the time required to reach 2σ detection significance for the hadronic showers. We consider DM signals from different models described in the text. We take the effective volume to be $V_{\rm eff} = 0.02$ km^3.

	$\theta_{\max} = 50^\circ$	
	$N_{\rm sh}$	$t_{\rm sh}$ (yr)
$\psi_{3/2} \to l^+l^-\nu$	11	23
$\psi_{3/2} \to (Wl, Z\nu, \gamma\nu)$	7	56
$\chi \to \mu^+\mu^-$	20	7
$B^{(1)}B^{(1)} \to (q\bar{q}, l^+l^-, \nu\bar{\nu}, \ldots)$	15	12
$\chi\chi \to \mu^+\mu^-$	68	0.64
ATM	676	

TABLE VI. Summary of the results for the event rates and the time that it takes to reach the 2σ effect for different values of m_χ and $\theta_{\max}$, where the threshold energy is taken as 50 GeV for both muon and shower events. In this table we do not include results which have $t > 15$ years for all m_χ. Results for the specific choice of the parameters in each model corresponding to fitting PAMELA, FERMI/LAT and HESS data are presented in red italic fonts.

		m_χ (TeV)									
		0.2	0.4	0.6	0.8	1	2	4	6	8	10
$\psi_{3/2} \to l^+ l^- \nu$	N_μ^{ct} (50°)	4.94	*11.15*	13.8	15.3	16.2	18.1	19.0	19.3	19.5	19.6
$B_\tau = 2.3$	$N_\mu^{\rm up}$ (50°)	8.68	*59.5*	120	180	239	503	912	1228	1485	1704
	$N_{\rm sh}$ (50°)	4	*11*	13	15	16.3	19	21	22	22	22
	$t_\mu^{\rm up}$ (10°)	1.3×10^4	*277*	69	30	17	4	1.2	0.7	0.5	0.4
	$t_\mu^{\rm up}$ (50°)	3490	*74*	18	8	5	1	0.32	0.18	0.12	0.09
	$t_{\rm sh}$ (50°)	196	*23*	16	12	10	7	6.3	5.8	5.8	5.8
$\psi_{3/2} \to (Wl, Z\nu, \gamma\nu)$	N_μ^{ct} (50°)	6.1	*8.4*	8.9	9.1	9.15	9.2	9.2	9.2	9.2	9.2
$B_\tau = 2.3$	$N_\mu^{\rm up}$ (50°)	9.9	*50.9*	95.6	139	181	364	638	844	1010	1150
	$N_{\rm sh}$ (50°)	3.6	*7.66*	9.6	10.74	11.5	13.17	14.12	14.46	14.64	14.74
	$t_\mu^{\rm up}$ (10°)	1×10^4	*378*	107	51	30	7.5	2.5	1.4	1	0.8
	$t_\mu^{\rm up}$ (50°)	2693	*101*	29	14	8	2	0.7	0.4	0.3	0.2
	$t_{\rm sh}$ (50°)	210	*47*	30	24	21	16	14	13	13	13
$\chi \to \mu^+ \mu^-$	N_μ^{ct} (50°)	2.13	6.45	8.43	9.5	10.2	*11.5*	12.2	12.4	12.5	12.6
$B_\tau = 2.9$	$N_\mu^{\rm up}$ (50°)	3.14	29	62.3	97	131	*286*	533	728	886	1022
	$N_{\rm sh}$ (50°)	1.95	8.22	12.09	14.55	16.2	*20.2*	22.45	23.27	23.68	23.94
	$t_\mu^{\rm up}$ (10°)	1×10^5	1×10^3	252	104	57	*12*	3.5	1.9	1.3	0.97
	$t_\mu^{\rm up}$ (50°)	2.6×10^4	316	68	28	15	*3.2*	0.93	0.5	0.34	0.26
	$t_{\rm sh}$ (50°)	709	40	19	13	11	*6.9*	5.5	5.2	5	4.8
$B^{(1)} B^{(1)} \to \ldots$	N_μ^{ct} (10°)	14.2	9.8	7.2	*5.6*	4.6	2.4	1.25	0.84	0.63	0.51
$B = 200$	$N_\mu^{\rm up}$ (10°)	86.1	131	140	*130*	128	124	108	92	81	72
	$N_{\rm sh}$ (10°)	11	9	7	*5.7*	4.8	2.6	1.4	0.9	0.7	0.6
	$t_\mu^{\rm up}$ (1°)	1.27	0.63	0.54	*0.65*	0.66	0.7	0.87	1.14	1.42	1.72
	$t_\mu^{\rm up}$ (10°)	1.55	0.68	0.57	*0.71*	0.72	0.76	1.0	1.36	1.76	2.2
	$t_\mu^{\rm up}$ (50°)	5.1	2.2	1.84	*2.29*	2.3	2.44	3.2	4.5	5.8	7.2
	$t_{\rm sh}$ (1°)	3.4	4.4	5.9	*7.7*	9.6	22	61	116	189	280
	$t_{\rm sh}$ (10°)	1.3	1.9	2.9	*4.3*	5.8	18	64	136	237	364
	$t_{\rm sh}$ (50°)	3.3	5	8	*12*	16.3	57	204	445	777	1202
$\chi\chi \to \mu^+ \mu^-$	N_μ^{ct} (10°)	40.19	29.58	22.01	17.39	*14.3*	7.59	3.90	2.63	1.98	1.59
$B = 400$	$N_\mu^{\rm up}$ (10°)	144	241	273	283	*320*	266	221	190	167	151
	$N_{\rm sh}$ (10°)	51.4	45.6	36.4	30	*25*	14	7.4	5	3.8	3
	t_μ^{ct} (1°)	1.11	1.68	2.55	3.61	*4*	13.64	44	92	156	238
	t_μ^{ct} (10°)	0.66	1.18	2.06	3.24	*4.7*	16.31	61	133	234	364
	t_μ^{ct} (50°)	1.93	3.55	6.38	10.2	*15*	53	201	444	781	1213
	$t_\mu^{\rm up}$ (1°)	0.54	0.24	0.2	0.18	*0.14*	0.21	0.28	0.35	0.43	0.50
	$t_\mu^{\rm up}$ (10°)	0.47	0.21	0.16	0.15	*0.12*	0.17	0.25	0.33	0.42	0.52
	$t_\mu^{\rm up}$ (50°)	1.83	0.65	0.51	0.47	*0.37*	0.54	0.78	1.1	1.35	1.7
	$t_{\rm sh}$ (1°)	0.63	0.72	0.91	1.12	*1.37*	2.58	5.5	9	13	18
	$t_{\rm sh}$ (10°)	0.12	0.14	0.2	0.26	*0.34*	0.87	2.63	5.34	9	13.6
	$t_{\rm sh}$ (50°)	0.18	0.22	0.33	0.48	*0.7*	2.1	7.2	15.5	27	42
Atmospheric	N_μ^{ct}	2.28 (1°)			227.5 (10°)				5347 (50°)		
	$N_\mu^{\rm up}$	28 (1°)			2794 (10°)				65668 (50°)		
	$N_{\rm sh}$	0.3 (1°)			28.8 (10°)				676 (50°)		

In what follows we consider cone half angles larger than $\theta_{\max} = 1°$. In Fig. 12, the detection times required for the signal s to satisfy Eq. (10) for the Kaluza-Klein and leptophilic annihilation cases are shown as a function of cone half angle. The optimal angle depends on the model and is of the order of a few degrees. The observation time is almost independent on the cone half angle in the range of a few degrees to about 10 degrees, but it increases for larger cone half angles where the signal increases slower than the background.

As shown in Fig. 13 for the decaying DM models, the observation time to reach the same significance decreases

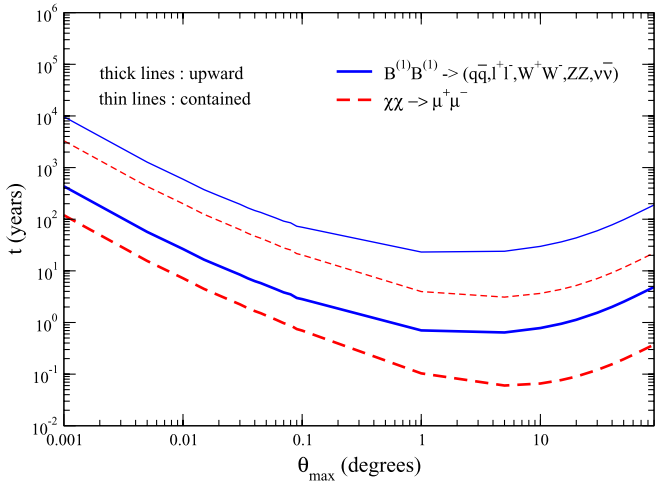

FIG. 12 (color online). The observation time t versus cone half angle $\theta_{\max}$ centered at the Galactic center to reach 2σ detection significance for the upward and contained muon events produced by the muon neutrinos originated from the annihilation of DM particles. Kaluza-Klein (solid lines) and leptophilic where $\chi\chi \to \mu^+\mu^-$ (dashed lines) models are considered. We take $E_\mu^{\rm th} = 50$ GeV.

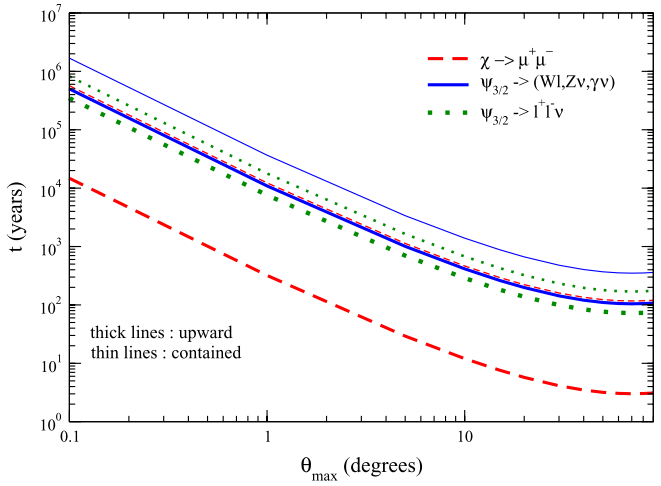

FIG. 13 (color online). The observation time t versus cone half angle $\theta_{\max}$ centered at the Galactic center to reach 2σ detection significance for the upward and contained muon events produced by the muon neutrinos originated from the decaying DM particles. Decay of leptophilic where $\chi \to \mu^+\mu^-$ (dashed lines), two-body decay (solid lines) and three-body decay (dotted lines) of gravitino are considered. We take $E_\mu^{\rm th} = 50$ GeV.

with the cone half angle $\theta_{\max}$, for $\theta_{\max} < 50°$, and it increases only slowly for the higher cone sizes, as the signal in directions away from the Galactic center are relatively more important.

We find that it takes, in general, a shorter amount of time for the upward muon events than the contained muon ones to reach the desired detection significance. It is mostly because of the small effective volume of the detector for contained events which results in lower event rates. The background is also small in this situation, however, still longer observation times are required due to low statistics. Among all the decaying DM models that we consider, the leptophilic model ($\chi \to \mu^+\mu^-$) seems most promising for detection of DM signal at 2σ level for $\theta_{\max} > 20°$ via upward muon events within a few years of observation.

C. Hadronic and electromagnetic showers

In addition to muons, the showers (hadronic and/or electromagnetic) produced in neutrino interactions could be used as signals of DM. The shower flux is given by [43]

$$\frac{d\phi_{\rm sh}}{dE_{\rm sh}} = \int_{E_{\rm sh}}^{E_{\max}} dE_\nu \left(\frac{d\phi_\nu}{dE_\nu}\right)\frac{N_A\rho}{2} \times \left(\frac{d\sigma_\nu^p(E_\nu, E_\nu - E_{\rm sh})}{dE_{\rm sh}} + (p \to n)\right) + (\nu \to \bar{\nu}), \quad (11)$$

where $d\sigma^{p,n}/dE_{\rm sh}$ is the differential cross section for showers produced in neutrino and antineutrino charged-current and neutral-current interactions with protons and neutrons.

In Fig. 14. we show shower flux for the case when the DM particle is a Kaluza-Klein particle, a gravitino and for a leptophilic model, for the model parameters listed in Table II. We take the cone half angle around the Galactic center to be $\theta_{\max} = 50°$. The shapes of the shower fluxes are similar to the contained muon fluxes presented in Fig. 4. The "golden channel", $\chi\chi \to \nu\bar{\nu}$, as in the case

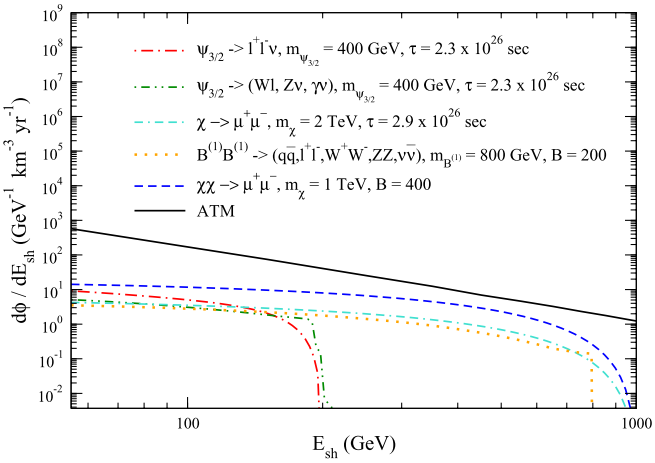

FIG. 14 (color online). Flux for the shower events for two-body (dot-dot-dashed line) and three-body (dot-dashed line) gravitino decay, decaying leptophilic model (dash-dash-dotted line), Kaluza-Klein annihilation (dotted line) and annihilating leptophilic model (dashed line) compared with the atmospheric background (solid line), for the case when $\theta_{\max} = 50°$. Model parameters are given in Table II.

of contained muons, contributes to the shower events at the highest kinematically allowed energy for the case when the DM particle is a Kaluza-Klein particle (dotted line) and when it is a gravitino (dot-dot-dashed line). While for the case of contained muons (Fig. 4), the DM signal in models with annihilating DM (Kaluza-Klein and leptophilic) exceeded the atmospheric background at high energies, shower signals for the same models are below the background. In addition, shower signals for the models in which DM annihilate are comparable to those in which DM decays. This is mainly due to our choice of large $\theta_{\rm max}$ for the showers ($\theta_{\rm max} = 50°$). This can be seen by comparing $\langle J_2\rangle_\Omega$ (for DM annihilation) and $\langle J_1\rangle_\Omega$ (for DM decay) given in Appendix A (Eq. (A3)) for different values of the cone size. For example, $\langle J_2\rangle_\Omega/\langle J_1\rangle_\Omega = 75$ for $\theta_{\rm max} = 1°$ whereas $\langle J_2\rangle_\Omega/\langle J_1\rangle_\Omega = 3$ for $\theta_{\rm max} = 50°$. Furthermore, shower fluxes extend to higher energies for the models in which DM annihilates than the case of DM decay, due to the kinematic constraints.

We evaluated the shower rates by integrating Eq. (11) over the shower energies

$$N_{\rm sh}(m_\chi) = \int_{E_{\rm sh}^{\rm th}}^{E_{\rm max}} \frac{d\phi_{\rm sh}}{dE_{\rm sh}} V_{\rm eff}(E_{\rm sh}) dE_{\rm sh}, \qquad (12)$$

where $V_{\rm eff}(E_{\rm sh})$ is the effective volume of the detector for measuring showers.

In Table V, we present the shower rates for a cone size of $\theta_{\rm max} = 50°$ for the DM models shown in Fig. 14. For the detector volume, we use an energy independent IceCube/DeepCore volume whose value is $V_{\rm eff} = 0.02$ km^3 for the showers [27,40,44]. The detector threshold is again set to be $E_{\rm sh}^{\rm th} = 50$ GeV. Although the number of events for all models is relatively small compared to the atmospheric background, the number of years needed for detection of the 2σ effect is encouraging for the leptophilic model as seen in Table V. We note that showers seem to be the best way to look for the signal of decaying DM.

The shower event rates depend on the DM decay time and the boost factor as an overall normalization while the dependence on DM mass is nontrivial. In order to illustrate shower event rate dependence on the DM mass, we take fixed boost factor or fixed decay time used in Fig. 14 for the annihilating (decaying) DM models and we obtain shower rates for different m_χ. From Fig. 15 we note that the shower event rate dependence on m_χ has similar behavior to the case of contained muon events (see Fig. 7), due to the similar flux of showers and muons in neutrino charged-current and neutral-current interactions. For the case when the DM is a Kaluza-Klein particle or in the leptophilic ($\chi\chi \to \mu^+\mu^-$) model the shower rates decrease with the DM mass while for the decaying DM models it is slowly increasing with m_χ for $m_\chi < 1$ TeV and become almost m_χ independent for higher values of m_χ. For the shower events, the differential weak scattering cross section in Eq. (11) becomes higher for low shower energies so that the rates for the showers tend to increase more than those for the muons as the energy decreases. Consequently, the dependence on the choice of the detector threshold becomes more significant for the DM masses close to the threshold energy. We also note that within the cone half angle of 50° and with the chosen model parameters the rates for showers due to decaying DM models are comparable to those for the annihilating DM models. For $m_\chi > 1$ TeV ($m_\chi > 4$ TeV), the shower rates for decaying DM models are larger than for the Kaluza-Klein (leptophilic where $\chi\chi \to \mu^+\mu^-$) model.

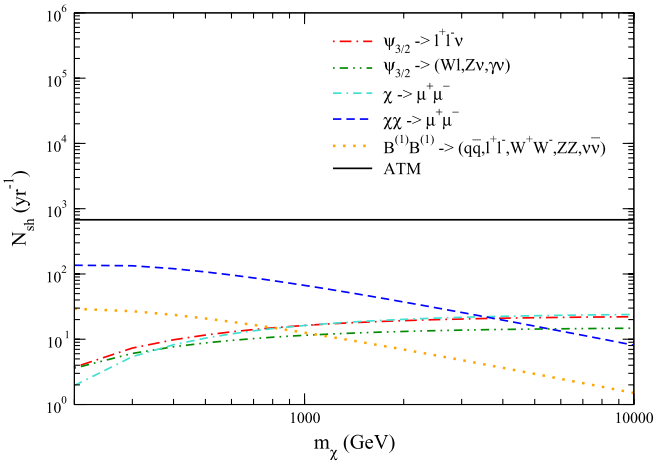

FIG. 15 (color online). Shower event rates as a function of DM mass for models considered in Table II. The boost factors for annihilating DM models and the decay times for the decaying DM models are fixed to the values in Table II. We take $\theta_{\rm max} = 50°$ and $E_{\rm sh}^{\rm th} = 50$ GeV.

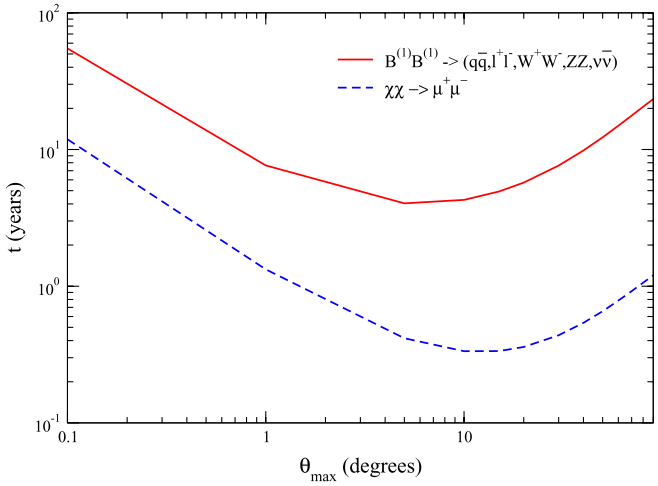

FIG. 16 (color online). The time t versus cone half angle $\theta_{\rm max}$ centered at the Galactic center to reach 2σ detection significance for the hadronic showers produced by the neutrinos from $\chi\chi \to \mu^+\mu^-$ (dashed line) and from the Kaluza-Klein DM particle (solid line). We take $E_{\rm sh}^{\rm th} = 50$ GeV.

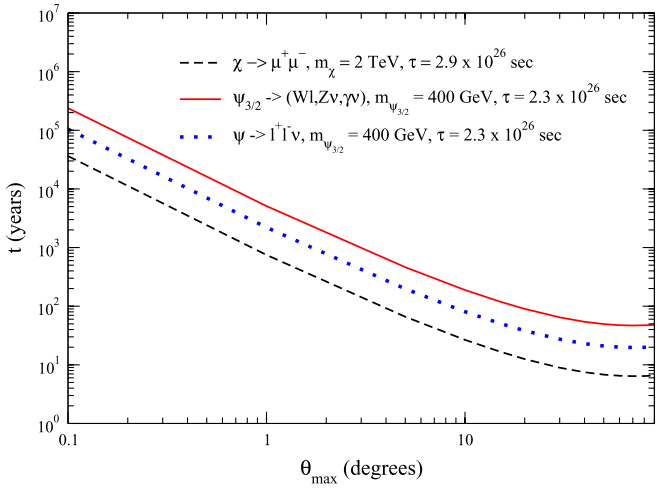

FIG. 17 (color online). The time t versus cone half angle $\theta_{\max}$ centered at the Galactic center to reach 2σ detection significance for the hadronic showers produced by the neutrinos from $\chi \rightarrow \mu^+\mu^-$ (dashed line) and from the two-body (solid line) and three-body (dotted line) decay models of gravitino. We take $E_{\rm sh}^{\rm th} = 50$ GeV.

The time required for the shower signal to be at 2σ level for different values of the cone half angle centered at the Galactic center is presented in Fig. 16 for the Kaluza-Klein DM particle (solid line) and for leptophilic model (dashed line) as an example for annihilating and decaying DM models. We find that the optimum time is for the cone half angle of 4°–10°. For the leptophilic model, one could reach the 2σ signal within few months of observation for $\theta_{\max} = 10°$. In the case of the Kaluza-Klein DM particle, one needs about 4 years of data taking for $\theta_{\max} = 4°$. For comparison, in Fig. 17 we show the time needed for detection of 2σ signal for the leptophilic model when a DM particle decays (dashed line), and for gravitino two-body (solid line) and three-body decay (dotted line) models. The optimum angle for decaying DM models is about 50°. This is similar to the previously discussed muon signal presented in Fig. 13, but shower signals seem to be better for possible detection of the gravitino. This is because of better statistics with the increase in the cone half angle and also the inclusion of the contributions from the charged-current and neutral-current interactions of the tau neutrinos and electron neutrinos with the detector medium. We note, however, that the 20 years required for $\theta \geq 50°$ for these parameters is not feasible in practice.

In Fig. 18, we present results for DM annihilation cross section required for a given DM mass in order to reach 2σ detection significance with shower events in five years of observation within $\theta_{\max} = 1°$. From Fig. 15 we note that the shower event rates decrease with m_χ for annihilating DM particles for a fixed annihilation cross section, therefore the curves for DM annihilation cross section versus DM mass in Fig. 18 increase in order for reach 2σ effect for a given m_χ. The parameter space above the curves defines the exclusion region and the leptophilic model seems to be more constrained than the Kaluza-Klein model. For the decaying DM models, our results for shower event rates obtained with fixed decay times (Fig. 15) indicate that the 2σ detection significance in 5-yr curves for the decay time versus DM mass should increase with m_χ for $m_\chi < 1$ TeV and becomes almost flat for $m_\chi > 1$ TeV. This is shown in Fig. 19. In this case, the exclusion regions for the model parameters, decay time and the mass, at 2σ level in five years, are the regions below the curves. For the leptophilic models with parameters that satisfy Eq. (2), 2σ signal detection would imply

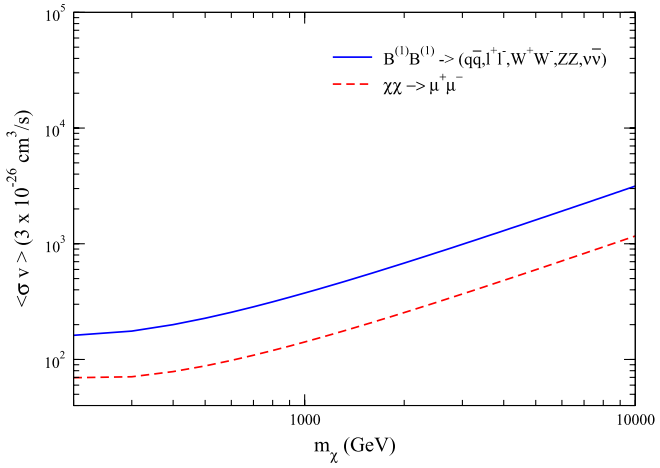

FIG. 18 (color online). Annihilation cross section versus DM mass for shower events to reach 2σ detection significance after five years of observation for the case of Kaluza-Klein (solid lines) and leptophilic (dashed lines) models. We take $\theta_{\max} = 50°$ and $E_{\rm sh}^{\rm th} = 50$ GeV.

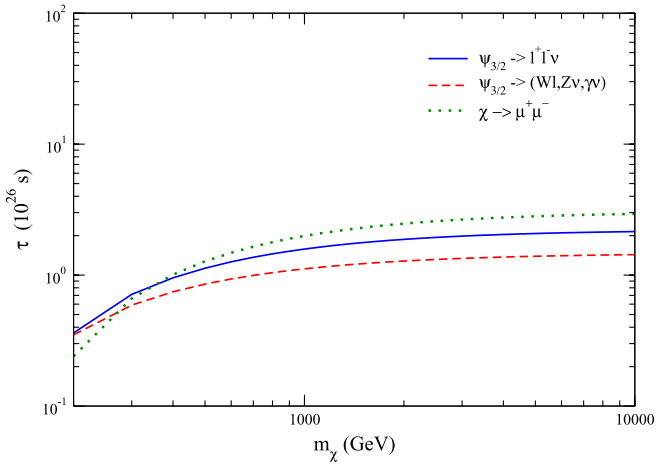

FIG. 19 (color online). Decay time versus DM mass for both shower events to reach 2σ detection significance after five years of observation for the case of decaying DM models: gravitino three-body (solid lines), gravitino three-body (dashed lines) and leptophilic (dotted lines). We take $\theta_{\max} = 50°$ and $E_{\rm sh}^{\rm th} = 50$ GeV.

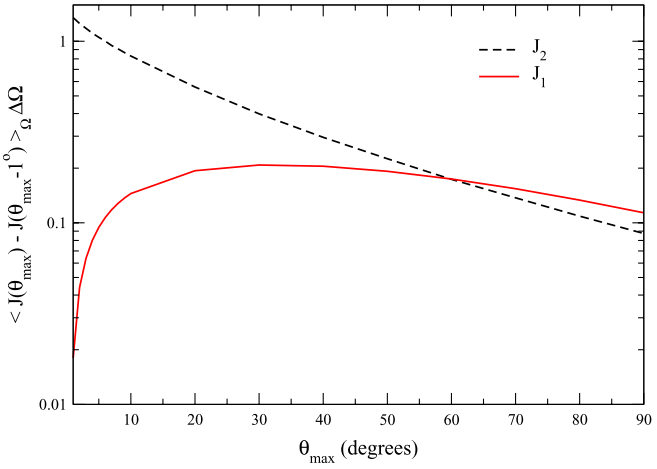

FIG. 20 (color online). J factor values both for annihilating (dashed line) and decaying (solid line) DM models for a wedge between $\theta_{\max} - 1°$ and $\theta_{\max}$ about the Galactic center as a function of $\theta_{\max}$.

that the DM particle mass is 250 GeV in the case of the annihilating DM, while for the case of the decaying leptophilic DM the DM mass would be 3 TeV.

V. CONCLUSIONS

We have studied neutrino signals from DM annihilation and decay in the Galactic center assuming an NFW profile as the DM density distribution in the Galaxy. We have considered models in which the DM particle is a gravitino, a Kaluza-Klein particle and a particle in a leptophilic model. In the case of the leptophilic model, we have considered both the case of decaying and annihilating DM. For a gravitino, we have taken into account both two-body and three-body decay channels. For each DM model, we have calculated contained and upward muons and showers using the model parameters that were obtained by fitting the excesses in the γ-ray and in the positron or electron plus positron data from the observations of HESS, PAMELA and FERMI/LAT. We have used a range of cone half angles for the muon and shower events, and we have studied the dependence on the choice of the cone size and DM mass.

Our results are summarized in Table VI. The specific models which are designed to account for the lepton excesses, listed in Table II, are indicated by the italic entries (highlighted in red in the online version). In addition, in Table VI, we show the event rates and time required for a 2σ observation for a range of masses and several values of $\theta_{\max}$. Note that the event rates for different $\theta_{\max}$ can be obtained by using a rescaling of J-factors, for example $J_1(50°)/J_1(10°) = 9$ and $J_1(10°)/J_1(1°) = 50$ for decaying dark matter models; $J_2(50°)/J_2(10°) = 2.7$ and $J_2(10°)/J_2(1°) = 7.2$ for annihilating dark matter models. In Table VII one can find the values of $J(\theta_{\max})$.

TABLE VII. The values of J factors for NFW profile for $\theta_{\max} = 0.1°, 1°, 5°, 25°, 50°, 70°, 90°$.

	0.1°	1°	5°	25°	50°	70°	90°
$\langle J_2\rangle_\Omega \Delta\Omega$	0.14	1.35	5.94	19.68	27.75	31.73	33.42
$\langle J_1\rangle_\Omega \Delta\Omega$	0.00027	0.018	0.30	3.69	8.79	12.24	14.90

For the leptophilic model ($\chi\chi \to \mu^+\mu^-$), for example, with $m_\chi = 1$ TeV and $B = 400$, the muon flux due to DM annihilation dominates over muons produced by the atmospheric neutrinos, for the muon energies in the range, 200 GeV $< E_\mu <$ 950 GeV (50 GeV $< E_\mu <$ 750 GeV) for the contained (upward) muon events with cone half angle $\theta_{\max} = 1°$. The shower event rates for this same model never exceed the atmospheric neutrino induced shower rates, for $\theta_{\max} = 50°$, in part due to the cone size.

For $m_\chi = 800$ GeV, $B = 200$ and $\theta_{\max} = 1°$, the contained muon flux due to annihilating Kaluza-Klein particles becomes larger than the background for $E_\mu >$ 300 GeV and up to the kinematic cutoff $E_\mu = m_\chi =$ 800 GeV. The muon flux is comparable to the background for muon energies 200 GeV $< E_\mu <$ 400 GeV for the upward muons.

With the model parameters that we considered, the decaying DM models do not produce the muon signal (upward or contained) that is above the atmospheric background. The muon flux from the decaying DM would be comparable to those for the annihilating DM models only if the decay times were of the order $\sim 10^{25}$ sec and $\sim 10^{24}$ sec for contained muon and upward muon events, respectively. In contrast to the muon case, we find that for a wide range of shower energies, the shower flux for decaying leptophilic particle ($\chi \to \mu^+\mu^-$) is larger than for the annihilating Kaluza-Klein particle.

We have also calculated the total muon and shower event rates by folding the corresponding fluxes with the energy independent IceCube/DeepCore effective volume, i.e. $V_{\rm eff} = 0.04(0.02)$ km^3 for the contained muon (shower) events. Because of its location the IceCube detector is unable to study the upward muons produced by the neutrinos coming from the Galactic center. However, we have calculated the upward muon rates for the IceCube-type detector in the Northern hemisphere by folding the muon fluxes with a muon effective area, which is assumed to be $A_{\rm eff} = 1$ km^2.

Even if there is a significant signal to background ratio, low statistics may yield difficulties in confirming the presence of a DM signal via neutrinos. Thus, we have evaluated how many years it would take to observe a 2σ effect. Using our results for the muon and shower event rates, we have also obtained the contour exclusion plots in which we show the regions for the model parameter space for each DM model in the case of no signal detection at 2σ detection significance in five years.

We find that the leptophilic model ($\chi\chi \to \mu^+\mu^-$) has stronger constraints on the DM annihilation cross section (or the boost factor) and m_χ than the case of the Kaluza-Klein particle. In terms of the constraint on the annihilation cross section, for the leptophilic DM model where the boost factor and DM mass are related by Eq. (2), after five years, the range of $m_\chi > 250$ GeV would be excluded by upward muon events for $A_{\rm eff} = 1$ km^2 and events within a cone half angle of $\theta_{\rm max} = 1^\circ$. A similar limit is obtained from the shower rate as well. More generally, we find that the upward muon and the shower events are more constraining than the contained muon ones. If there is no upward muon signal detected in five years, with $\theta_{\rm max} = 10^\circ$, for the decaying leptophilic model ($\chi \to \mu^+\mu^-$) which satisfies the constraint given by Eq. (2), m_χ is constrained to be smaller than 3 TeV.

In our calculations, we have taken the detector muon and shower energy thresholds to be 50 GeV. Changing the detector threshold energy to about 100 GeV does not affect our results significantly. However, decreasing the threshold energy down to $\sim$10 GeV results in a larger atmospheric background relative to the DM signal. Consequently, detecting a DM signal via muon or shower events with low detector thresholds ($\sim$ 10 GeV) becomes more difficult.

Increasing the cone half angle, $\theta_{\rm max}$ about the Galactic center increases the DM signal, however it does not necessarily improve the detection significance since the background signal due to atmospheric neutrinos is also enhanced. We have found the optimum cone half angles for all types of events in order to reach the 2σ detection level. For the annihilating DM models, we have found the optimum angle to be a few degrees for the muon events and about 10° for the shower events. In both cases, we have shown that there is a good chance of detecting both leptophilic and Kaluza-Klein particles in less than ten years for some DM masses.

In the case of the decaying DM models, the optimum angle is about 50° for both muons and showers. For gravitino DM, signals could be detected in ten years only with shower events, while the decaying leptophilic particle can be detected with upward muon events as well in a few years.

Our results with fixed annihilation cross section or decay time and variable DM mass can be used to predict neutrino signals for any other values for the parameters of the models we consider. For example, in the literature, the HESS data is also explained by a hypothetical Kaluza-Klein particle with mass $m_\chi = 10$ TeV [14]. The boost factor that is required, in this case, is $B = 1000$. By rescaling the results in the previous sections, we find that the observation time to reach 2σ detection significance becomes 0.1 years for the upward muon events. For contained muons and showers, it is not feasible to detect the 2σ effect within reasonable time ($t \gg 20$ years). Increasing the boost factor by a factor of 5 and the DM mass by a factor of about 10 relative to the parameters of Table II significantly improves the chance for detecting the Kaluza-Klein particle via upward muon events.

Similar to the decaying leptophilic model, the gravitino model ($\psi_{3/2} \to l^+ l^- \nu$) with a gravitino mass of 3.3 TeV and decay time $\tau = 5 \times 10^{25}$ sec can also account for the FERMI data [17]. For a decaying DM particle, increasing the DM mass (for a fixed decay time) increases the event rates. Since the neutrino flux scales as $\sim\tau^{-1}$ (see Eq. (A2)), decreasing the decay time also enhances the neutrino signals for a decaying DM particle. Therefore, a combination of higher mass and shorter decay time should increase all the event rates that we have calculated for a lighter ($m_{\psi_{3/2}} = 400$ GeV) gravitino particle which has a longer decay time ($\tau = 2.3 \times 10^{26}$ sec). For the model parameters, $m_\chi = 3.3$ TeV and $\tau = 5 \times 10^{25}$ sec , we find that the 2σ detection significance can be reached in 2.6 years via upward muons and in less than a year via the hadronic showers. In addition, for the contained muons the observation time decreases by 2 orders of magnitude relative to the value given in Table IV.

The dependence of the signal on the cone half angle is different for the annihilating DM particles than for the decaying DM particles. We have demonstrated this by choosing wedges between $\theta_{\rm max} - 1^\circ$ and $\theta_{\rm max}$ centered at the Galactic center and calculating $\langle J_n\rangle_\Omega \Delta\Omega$, which defines an overall normalization for the neutrino signals, for different $\theta_{\rm max}$ for both annihilating and decaying DM particles. The angular wedges can be used to rescale event rates as well. Our results indicate that the J factor for the annihilating DM particle decreases sharply with $\theta_{\rm max}$ whereas for the case of the decaying DM particle, for a wide range of $\theta_{\rm max}$, the J factor has a weak $\theta_{\rm max}$ dependence. In determining the nature of the DM (annihilating or decaying), the directional dependence of the neutrino signals gives valuable information.

ACKNOWLEDGMENTS

M. H. R. thanks the members of the Center for Cosmology and Astroparticle Physics at The Ohio State University for their hospitality. This research was supported by U.S. Department of Energy Contracts DE-FG02-91ER40664, DE-FG02-04ER41319 and DE-FG02-04ER41298.

APPENDIX A: NEUTRINO FLUX

The neutrino flux observed at the Earth due to the DM annihilation or decay in the galaxy for a given neutrino flavor can be written as [22]

$$\frac{d\phi_\nu}{dE_\nu} = R_o \rho_o^2 B \frac{\langle\sigma v\rangle}{8\pi m_\chi^2}\left(\sum_F B_F \frac{dN_\nu^F}{dE_\nu}\right)\langle J_2\rangle_\Omega \Delta\Omega \qquad \text{(A1)}$$

for the case of annihilating DM, and

$$\frac{d\phi_\nu}{dE_\nu} = R_o \rho_o \frac{1}{4\pi m_\chi \tau}\left(\sum_F B_F \frac{dN_\nu^F}{dE_\nu}\right)\langle J_1\rangle_\Omega \Delta\Omega \qquad \text{(A2)}$$

for the case of decaying DM where dN_ν^F/dE_ν is the neutrino spectrum for a given annihilation or decay channel F with branching fraction B_F, B is the boost factor, τ is the decay time, R_o is the distance of the solar system from the Galactic center and ρ_o is the local density near the solar system. The neutrino energy spectrum, dN_ν^F/dE_ν for different channels can be found in Appendix B. In the above equations, the dimensionless quantity $\langle J_n\rangle_\Omega$ is defined as [12,22,26]

$$\langle J_n\rangle_\Omega = \int \frac{d\Omega}{\Delta\Omega}\int_{\text{l.o.s}} \frac{dl(\theta)}{R_o}\left(\frac{\rho(l)}{\rho_o}\right)^n, \qquad \text{(A3)}$$

where $\rho(l)$ is the DM density, $l(\theta)$ is the distance between the source and the Earth in the direction of θ which is the cone half angle from the Galactic center and the integral is over the line of sight (l.o.s.) within a solid angle $\Delta\Omega = 2\pi(1 - cos\theta_{\max})$, centered in the Galactic center.

In our calculations, we take the DM annihilation cross section to have the typical thermal relic value $\langle\sigma v\rangle = 3 \times 10^{-26}\ \text{cm}^3\,\text{s}^{-1}$ and we use the Navarro-Frenk-White (NFW) DM density profile [33]

$$\rho(r) = \frac{\rho_s}{(r/R_s)(1 + r/R_s)^2}, \qquad \text{(A4)}$$

where ρ_s and R_s are the parameters which vary from halo to halo. In our calculations we set $\rho_s = 0.2589\ \text{GeV/cm}^3$ and $R_s = 20$ kpc so that the DM density in the vicinity of the solar system ($r = R_o = 8.5$ kpc) takes the typical value $\rho(R_o) = 0.3\ \text{GeV/cm}^3$ [45]. Using these definitions, we can write $r = \sqrt{R_o^2 + l^2 - 2R_o l\cos\theta}$ and the upper limit for the l integral in Eq. (A3) can be obtained as $l_{\max} = R_o\cos\theta + \sqrt{R_s^2 - R_o^2\sin^2\theta}$ for a given θ.

For the NFW profile, some values for $\langle J_2\rangle_\Omega\Delta\Omega$ and $\langle J_1\rangle_\Omega\Delta\Omega$ are summarized in Table VII.

In Fig. 20 we show $\langle J_n\rangle_\Omega\Delta\Omega$ factors as a function of $\theta_{\max}$ for DM annihilation ($n = 2$) and DM decay ($n = 1$) evaluated for a cone wedge between $\theta_{\max} - 1^\circ$ and $\theta_{\max}$ around the Galactic center.

APPENDIX B: NEUTRINO SPECTRA

In this study, we have studied the model dependent neutrino signals from the annihilation/decay of the DM particles that reside in the galaxy. We assumed that the DM particles are nonrelativistic so that their total energy is close to their rest energy ($E_\chi \simeq m_\chi$). The neutrinos with energy E_ν can be produced from the annihilation/decay of the DM or from the decay of quarks, charged leptons and gauge bosons which are produced by the annihilation/decay of the DM. In our calculations, we have used the standard unpolarized decay distributions which, in general, take one of the following forms:

$$\frac{dN}{dx} = 2B_f(3x^2 - 2x^3) \qquad \text{(B1)}$$

$$\frac{dN}{dx} = 12B_f(x^2 - x^3) \qquad \text{(B2)}$$

$$\frac{dN}{dx} = B_f\delta(x - 1) \qquad \text{(B3)}$$

in the rest frame of the decaying particle where $x = 2E_\nu/m_d$, m_d is the mass of the decaying particle and B_f is the decay branching fraction for a given decay channel. Once the distribution in the rest frame is known, the neutrino energy spectrum from a decaying particle with velocity β_d and energy $E_d = \gamma_d m_d$ is given by [46]

$$\left(\frac{dN_\nu}{dE_\nu}\right) = \frac{1}{2}\int_{E_-}^{E_+}\frac{d\epsilon}{\epsilon}\frac{1}{\gamma_d\beta_d}\left(\frac{dN}{d\epsilon}\right)^{\text{rest}}, \qquad \text{(B4)}$$

where $E_\mp = E_\nu\gamma_d^{-1}(1 \pm \beta_d)^{-1}$.

1. Neutrino spectrum from $\chi \to Z\nu$ decay channel

In our calculations, for the channel $\chi \to Z\nu$ we use the Breit-Wigner distribution given as [23]

$$\frac{dN_\nu}{dE_\nu} = \frac{1}{(E_\nu^2 - E_{\nu Z}^2)^2 + E_{\nu Z}^2\Gamma_{\nu Z}^2} \times\left(\int_0^\infty \frac{dE}{(E^2 - E_{\nu Z}^2)^2 + E_{\nu Z}^2\Gamma_{\nu Z}^2}\right)^{-1}, \qquad \text{(B5)}$$

where the distribution peaks at

$$E_{\nu Z} = \frac{m_\chi}{2}\left(1 - \frac{m_Z^2}{m_\chi^2}\right), \qquad \text{(B6)}$$

and

$$\Gamma_{\nu Z} = \frac{m_Z}{m_\chi}\Gamma_Z. \qquad \text{(B7)}$$

We take $\Gamma_Z = 2.5$ GeV.

2. Neutrino spectrum from $\tau^\mp$, $\mu^\mp$ decay channels

In this section, we present the ν_μ spectrum from μ and τ decays. The spectra for other neutrino flavors can be deduced from these results. For example, the ν_e spectrum from μ decay is identical to the ν_μ spectrum from τ decay and the ν_τ spectrum from τ decay to that of ν_μ from μ decay. For these three-body decays, the ν_μ spectrum from τ decay is given by Eq. (B2) and from μ decay by Eq. (B1) in the frame where the decaying particle is at rest. Then, after boosting these results by using Eq. (B4) for charged leptons produced via the DM annihilation or decay, we obtain

$$\frac{dN_{\nu_\mu}}{dE_{\nu_\mu}} = \begin{cases} \frac{B_f}{E_l}\left(\frac{5}{3} - 3x^2 + \frac{4}{3}x^3\right), & \mu \to \nu_\mu e \nu_e \\ \frac{2B_f}{E_l}\left(1 - 3x^2 + 2x^3\right), & \tau \to \nu_\tau \mu \nu_\mu, \end{cases} \tag{B8}$$

where $x = \frac{E_{\nu_\mu}}{E_l} \leq 1$ and $E_l = m_\chi$ for the case of annihilation or $E_l = m_\chi/2$ for the case of decay. The decay branching fraction, $B_f = 0.18(1)$ for $\tau(\mu)$ decay. In addition to the three-body decays, τ can also decay into ν_τ via $\tau \to \nu_\tau M$ or $\tau \to \nu_\tau X$ where $M = \pi$, ρ, a_1 mesons and X indicates hadrons. The neutrino spectra from these channels are given as [43]

$$\frac{dN_{\nu_\tau}}{dE_{\nu_\tau}} = \begin{cases} \frac{B_f}{E_\tau}\frac{1}{r_M} & \text{when } \frac{E_\nu}{E_\tau} < r_M \quad \text{for mesons} \\ \frac{0.13}{0.3E_\tau} & \text{when } \frac{E_\nu}{E_\tau} < 0.3 \quad \text{for hadrons,} \end{cases} \tag{B9}$$

where $r_M = 1 - m_M^2/m_\tau^2$ with m_M and m_τ being the mass of the meson M and the τ lepton, respectively. Here, $B_f = 0.12$, 0.26, 0.13 and $r_M = 0.99$, 0.81, 0.52 for $M = \pi$, ρ, a_1 respectively.

3. Neutrino spectrum from $b(\bar{b})$ and $c(\bar{c})$ decay channels

The b and c quarks hadronize before they decay into neutrinos. The hadronization effect is taken into account by scaling the initial quark energy, $E_{\rm in}$, in the form $E_f = z_f E_{\rm in}$, where $f = b$, c, $z_f = 0.73(0.58)$ for b (c) quarks [46] and $E_{\rm in} = m_\chi$ for an annihilating DM particle or $E_{\rm in} = m_\chi/2$ for a decaying DM particle with mass m_χ.

The neutrino spectrum from the decay of $f = b, \bar{b}, c$ or $\bar{c}$ from $\chi\chi \to f\bar{f}$ can also be approximated by the second equation in Eq. (B8) (see also [46,47]), i.e.,

$$\frac{dN_\nu}{dE_\nu} = \frac{2B_f}{E_f}(1 - 3x^2 + 2x^3) \quad \text{for } x \leq 1 = 0 \quad \text{otherwise,} \tag{B10}$$

where $x = \frac{E_\nu}{E_f}$ and

$$(E_f, B_f) = \begin{cases} (0.73E_{\rm in}, 0.103) & b \text{ channel} \\ (0.58E_{\rm in}, 0.13) & c \text{ channel.} \end{cases} \tag{B11}$$

4. $W^\mp$ and Z decay channels

In the $W^\mp$ and Z decay channels, the neutrino spectrum from the decaying particle with velocity, β_B, and energy, E_B, can be obtained by using Eqs. (B3) and (B4), i.e.,

$$\frac{dN_\nu}{dE_\nu} = \frac{n_f B_f}{E_B \beta_B} \quad \text{for } \frac{E_B}{2}(1 - \beta_B) < E_\nu < \frac{E_B}{2}(1 + \beta_B) = 0 \quad \text{otherwise,} \tag{B12}$$

where

$$(n_f, B_f) = \begin{cases} (1, 0.105) & W \text{ channel,} \\ (2, 0.067) & Z \text{ channel.} \end{cases} \tag{B13}$$

5. Neutrino spectrum from $t(\bar{t})$ decay channel

The top quark decays into a W boson and a b quark ($t \to Wb$) with a branching fraction close to unity. Thus, the sum of neutrino spectra of W and b channels gives the required spectrum, i.e.,

$$\left(\frac{dN_\nu}{dE_\nu}\right)^{\rm rest}_{t\bar{t}} = \left(\frac{dN_\nu}{dE_\nu}\right)_{W^+W^-} + \left(\frac{dN_\nu}{dE_\nu}\right)_{b\bar{b}}. \tag{B14}$$

Then, boosting this expression yields the neutrino spectrum from top quarks moving with velocity β_t and energy $E_t = \gamma_t m_t$ [46],

$$\frac{dN_\nu}{dE_\nu} = \left(\frac{dN_\nu}{dE_\nu}\right)_W + \left(\frac{dN_\nu}{dE_\nu}\right)_b, \tag{B15}$$

where

$$\left(\frac{dN_\nu}{dE_\nu}\right)_W = \frac{B_W}{2\gamma_t\beta_t E_W \beta_W} \ln\frac{\min(E_+, \epsilon_+)}{\max(E_-, \epsilon_-)} \quad \text{if } \gamma_t(1 - \beta_t)\epsilon_- < E_\nu < \gamma_t(1 + \beta_t)\epsilon_+ = 0 \quad \text{otherwise,} \tag{B16}$$

and

$$\left(\frac{dN_\nu}{dE_\nu}\right)_b = \frac{B_b}{2\gamma_t\beta_t E_d} D_b[E_-/E_d, \min(1, E_+/E_d)] \quad \text{if } E_\nu < \gamma_t(1 + \beta_t)E_d = 0 \quad \text{otherwise,} \tag{B17}$$

where $B_W = 0.105$, $B_b = 0.103$, $\epsilon^\mp = E_W(1 \mp \beta_W)/2$, $E_\mp = E_\nu \gamma_t^{-1}(1 \pm \beta_t)^{-1}$ and $E_d = 0.73E_b$ with E_W, β_W and E_b being equal to their values in the top-quark rest frame, i.e.,

$$E_b = \frac{m_t^2 - m_W^2}{2m_t} \qquad E_W = \frac{m_t^2 + m_W^2}{2m_t} \qquad \beta_W = \frac{E_b}{E_W}. \tag{B18}$$

The function D_b is given by

$$D_b[m, n] = \frac{1}{3}\left[9(m^2 - n^2) - 4(m^3 - n^3) + 6\ln\left(\frac{n}{m}\right)\right]. \tag{B19}$$

6. Neutrino spectrum from $\psi_{3/2} \to l^+ l^- \nu$ decay channel

In the zero mass limit, the primary lepton (l^+ or l^- or ν) spectrum from the decay channel, $\psi_{3/2} \to l^+ l^- \nu$, can be approximated to be

$$\frac{dN_{l(\nu)}}{dE_{l(\nu)}} = \frac{60}{m_{\psi_{3/2}}} x^4(1-x) \quad \text{where } x = \frac{2E}{m_{\psi_{3/2}}} \leq 1, \tag{B20}$$

by using the results in [48]. In order to obtain the spectrum for the secondary neutrinos produced from the primary charged lepton decays, one can use

$$\frac{dN_\nu}{dE_\nu} = \int_{E_\nu}^{m_{\psi_{3/2}}/2} dE_l \left(\frac{1}{N_l}\frac{dN_l}{dE_l}\right)\left(\frac{dN_\nu}{dE_\nu}\right)_{l\to\nu}. \tag{B21}$$

Here, $\frac{dN_l}{dE_l}$ is the primary charged lepton spectrum given by Eq. (B20) and the spectra $(\frac{dN_\nu}{dE_\nu})_{l\to\nu}$ are given by Eqs. (B8) and (B9). Then, the secondary ν_μ spectrum is derived to be

$$\left(\frac{dN_{\nu_\mu}}{dE_{\nu_\mu}}\right) = \frac{5B_f}{m_{\psi_{3/2}}}(1 - 6x^2 + 8x^3 - 3x^4), \tag{B22}$$

from the primary μ decays and

$$\left(\frac{dN_{\nu_\mu}}{dE_{\nu_\mu}}\right) = \frac{6B_f}{m_{\psi_{3/2}}}(1 - 10x^2 + 20x^3 - 15x^4 + 4x^5), \tag{B23}$$

from the primary τ decays, requiring that $x \leq 1$ in each case where $x = 2E_\nu/m_{\psi_{3/2}}$. Finally, for the ν_τ spectrum from the primary τ decays accompanied with the meson/hadron production, we find

$$\left(\frac{dN_{\nu_\tau}}{dE_{\nu_\tau}}\right) = \frac{3B_f}{r_M m_{\psi_{3/2}}}\left(1 - \frac{5}{r_M^4}x^4 + \frac{4}{r_M^5}x^5\right), \tag{B24}$$

with the requirement $r_M > x$.

APPENDIX C: PARAMETRIZATIONS

1. Contained and upward muons

Our results for the contained muon fluxes given in Fig. 4 can be parametrized as

$$\begin{aligned}\frac{d\phi_\mu^{ct}}{dE_\mu} &= \left(\frac{B}{100}\right)\left(\frac{\langle J_2\rangle \Delta\Omega}{1.35}\right)\frac{\xi(x)}{(m_\chi/\text{TeV})^2} \\ \frac{d\phi_\mu^{ct}}{dE_\mu} &= \left(\frac{\tau}{10^{26}\ \text{sec}}\right)^{-1}\left(\frac{\langle J_1\rangle \Delta\Omega}{0.018}\right)\frac{\xi(x)}{(m_\chi/\text{TeV})}\end{aligned} \tag{C1}$$

for annihilation and decay processes, respectively. The upward muon fluxes presented in Fig. 6 can be parametrized as

$$\begin{aligned}\frac{d\phi_\mu^{\text{up}}}{dE_\mu} &= \left(\frac{B}{100}\right)\left(\frac{\langle J_2\rangle \Delta\Omega}{1.35}\right)\frac{1}{(m_\chi/\text{TeV})}\frac{C(x)\xi(x)}{(1+1.5\frac{E_\mu}{\text{TeV}})} \\ \frac{d\phi_\mu^{\text{up}}}{dE_\mu} &= \left(\frac{\tau}{10^{26}\ \text{sec}}\right)^{-1}\left(\frac{\langle J_1\rangle \Delta\Omega}{0.018}\right)\frac{C(x)\xi(x)}{(1+1.5\frac{E_\mu}{\text{TeV}})},\end{aligned} \tag{C2}$$

where $x = E_\mu/m_\chi$ for DM annihilation and $x = 2E_\mu/m_\chi$ for the DM decay. The functions $\xi(x)$ and $C(x)$ are fitted to our results for muon fluxes and parametrize as

TABLE VIII. The best fit parameter values for the contained muon fluxes for different DM models.

	$\psi_{3/2}$ (three-body)	$\psi_{3/2}$ (two-body)	$\chi \to \mu^+\mu^-$	$B^{(1)}B^{(1)} \to \cdots$	$\chi\chi \to \mu^+\mu^-$
a_1	16.651	−32.032	0.0554	2.5637	0.029
a_2	−16.642	32.04	−0.0472	−2.5470	−0.0012
a_3	−16.640	32.03	−0.0472	−2.5546	−0.0012
a_4	8.242	−15.93	−0.009 34	1.2381	− 0.11
a_5	−2.553	5.022	0.0254	−0.3780	0.11
a_6	0.423	−0.87	−0.0069	0.06929	− 0.027
$a_7(10^{-6})$	0	0	−0.0765	215.8	− 0.04

TABLE IX. Same as Table VIII but for the upward muon fluxes.

	$\psi_{3/2}$ (three-body)	$\psi_{3/2}$ (two-body)	$\chi \to \mu^+\mu^-$	$B^{(1)}B^{(1)} \to \cdots$	$\chi\chi \to \mu^+\mu^-$
a_1	1.251	1.292	−0.7716	−3.4381	−4.60
a_2	−1.239	−1.285	0.781	3.4847	4.67
a_3	−1.266	−1.296	0.747	3.3390	4.44
a_4	0.638	0.641	−0.341	−1.5573	−2.0
a_5	−0.203	−0.196	0.0918	0.4439	0.526
a_6	0.0364	0.032	−0.0132	−0.0694	−0.073
$a_7(10^{-6})$	0	0	0.45	41.47	3.6
a_8	0.3	0.3	1.5	1.2	1.5

TABLE X. The best fit parameter values for the shower fluxes for different DM models.

	$\psi_{3/2}$ (three-body)	$\psi_{3/2}$ (two-body)	$\chi \to \mu^+\mu^-$	$B^{(1)}B^{(1)} \to \cdots$	$\chi\chi \to \mu^+\mu^-$
a_1	−6.335	− 14.129	− 22.867	−8.765	−32.43
a_2	6.355	14.139	22.898	8.78	32.48
a_3	6.274	14.100	22.765	8.72	32.29
a_4	−2.991	−6.952	− 11.134	−4.25	−15.79
a_5	0.813	2.127	3.325	1.25	4.71
a_6	−0.099	−0.347	−0.5125	−0.189	−0.73
$a_7(10^{-3})$	−0.472	0	0	0	0

$$\xi(x) = a_1 + a_2 e^{-x} + a_3 x + a_4 x^2 + a_5 x^3 + a_6 x^4 + a_7 \ln(x)$$
$$C(x) = 1 + a_8 x, \tag{C3}$$

with the best fit values for the parameters given in Tables VIII and IX for the contained and upward muons, respectively.

The background muon flux from atmospheric neutrinos can be written in a parametric form as

$$\left(\frac{d\phi_\mu}{dE_\mu}\right)^{\rm ct}_{\rm ATM,avg} = 3186.2\left(\frac{E_\mu}{\rm GeV}\right)^{-2.062}\left(\frac{\Delta\Omega}{10^{-3}\ \rm sr}\right) \tag{C4}$$

in units of $\mathrm{GeV}^{-1}\,\mathrm{km}^{-3}\,\mathrm{yr}^{-1}$ for the contained muon events and

$$\left(\frac{d\phi_\mu}{dE_\mu}\right)^{\rm up}_{\rm ATM,avg} = 89.0\left(\frac{E_\mu}{\rm GeV}\right)^{-1.475}\left(\frac{\Delta\Omega}{10^{-3}\ \rm sr}\right) \tag{C5}$$

in units of $\mathrm{GeV}^{-1}\,\mathrm{km}^{-2}\,\mathrm{yr}^{-1}$ for the upward muon events.

2. Showers

Our results for shower flux presented in Fig. 14 can be parametrized as

$$\frac{d\phi_{\rm sh}}{dE_{\rm sh}} = \left(\frac{B}{100}\right)\left(\frac{\langle J_2\rangle\Delta\Omega}{27.75}\right)\frac{\xi(x)}{(m_\chi/100\ \mathrm{GeV})^2}$$
$$\frac{d\phi_{\rm sh}}{dE_{\rm sh}} = \left(\frac{\tau}{10^{26}\ \rm sec}\right)^{-1}\left(\frac{\langle J_1\rangle\Delta\Omega}{8.79}\right)\frac{\xi(x)}{(m_\chi/\mathrm{GeV})} \tag{C6}$$

for DM annihilation and DM decay processes, respectively. The best fit values for the parameters are given in Table X

The background shower flux from atmospheric neutrinos can be written in a parametric form as

$$\left(\frac{d\phi_{\rm sh}}{dE_{\rm sh}}\right)_{\rm ATM,avg} = 3.21\times 10^6\left(\frac{E_\mu}{\rm GeV}\right)^{-2.155}\left(\frac{\Delta\Omega}{2.24\ \rm sr}\right) \tag{C7}$$

in units of $\mathrm{GeV}^{-1}\,\mathrm{km}^{-3}\,\mathrm{yr}^{-1}$.

[1] See, e.g., D. N. Spergel *et al.* (WMAP Collaboration), Astrophys. J. Suppl. Ser. **148**, 175 (2003); M. Tegmark *et al.*, Phys. Rev. D **69**, 103501 (2004); A. G. Sanchez *et al.*, Mon. Not. R. Astron. Soc. **366**, 189 (2006); J. Einasto, arXiv:0901.0632.

[2] F. Zwicky, Helv. Phys. Acta **6**, 110 (1933); Astrophys. J. **86**, 217 (1937).

[3] See, e.g., G. B. Gelmini, Int. J. Mod. Phys. A **23**, 4273 (2008), and references therein.

[4] O. Adriani *et al.* (PAMELA Collaboration), Nature (London) **458**, 607 (2009); E. Mocchiutti *et al.*, arXiv:0905.2551.

[5] A. A. Abdo *et al.* (Fermi LAT Collaboration), Phys. Rev. Lett. **102**, 181101 (2009).

[6] F. Aharonian *et al.* (HESS Collaboration), Astron. Astrophys. **425**, L13 (2004); **508**, 561 (2009).

[7] See, e.g., P. J. Fox and E. Poppitz, Phys. Rev. D **79**, 083528 (2009); R. Harnik and G. D. Kribs, Phys. Rev. D **79**, 095007 (2009); Q. H. Cao, E. Ma, and G. Shaughnessy, Phys. Lett. B 673, 152 (2009); B. Kyae, J. Cosmol. Astropart. Phys. 07 (2009) 028; X. J. Bi, X. G. He, and Q. Yuan, Phys. Lett. B **678**, 168 (2009); S. Baek and P. Ko, J. Cosmol. Astropart. Phys. 10 (2009) 011; D. J. Phalen, A. Pierce, and N. Weiner, Phys. Rev. D **80**, 063513 (2009); H. S. Goh, L. J. Hall, and P. Kumar, J. High Energy Phys. 05 (2009) 097; A. Ibarra, A. Ringwald, D. Tran, and C. Weniger, J. Cosmol. Astropart. Phys. 08 (2009) 017; Y. Farzan, S. Pascoli, and M. A. Schmidt, arXiv:1005.5323.

[8] K.-Y. Choi, D. Restrepo, C. E. Yaguna, and O. Zapata, arXiv:1007.1728; J. M. Cline, A. C. Vincent, and W. Xue, Phys. Rev. D **81**, 083512 (2010).

[9] See, e.g., E. Nardi, F. Sannino, and A. Strumia, J. Cosmol. Astropart. Phys. 01 (2009) 043; A. Arvanitaki, S. Dimopoulos, S. Dubovsky, P. W. Graham, R. Harnik, and S. Rajendran, Phys. Rev. D **80**, 055011 (2009).

[10] A. Ibarra, D. Tran, and C. Weniger, J. Cosmol. Astropart. Phys. 01 (2010) 009.

[11] G. Bertone, W. Buchmuller, L. Covi, and A. Ibarra, J. Cosmol. Astropart. Phys. 11 (2007) 003; G. D. Mack, T. D. Jacques, J. F. Beacom, N. F. Bell, and H. Yuksel, Phys. Rev. D **78**, 063542 (2008); N. F. Bell and T. D. Jacques, Phys. Rev. D **79**, 043507 (2009); V. Barger, Y. Gao, W. Y. Keung, and D. Marfatia, Phys. Rev. D **80**, 063537 (2009); P. D. Serpico and D. Hooper, New J. Phys. **11**, 105010 (2009); G. Bertone, M. Cirelli, A. Strumia, and M. Taoso, J. Cosmol. Astropart. Phys. 03 (2009) 009; L. Bergstrom, G. Bertone, T. Bringmann, J. Edsjo, and M. Taoso, Phys. Rev. D **79**, 081303 (2009); S. Palomares-Ruiz and J. M. Siegal-Gaskins, J. Cosmol. Astropart. Phys. 07 (2010) 023.

[12] E. Athanassoula, F.-S. Ling, E. Nezri, and R. Teyssier, Astropart. Phys. **31**, 37 (2009).

[13] M. Cirelli, P. Panci, and P. D. Serpico, Nucl. Phys. **B840**, 284 (2010).

[14] L. Bergstrom, T. Bringmann, M. Eriksson, and M. Gustafsson, Phys. Rev. Lett. **94**, 131301 (2005).

[15] A. Ibarra and D. Tran, Phys. Rev. Lett. **100**, 061301 (2008).

[16] V. Barger, Y. Gao, W. Y. Keung, D. Marfatia, and G. Shaughnessy, Phys. Lett. B **678**, 283 (2009).

[17] B. Bajc, T. Enkhbat, D. K. Ghosh, G. Senjanovic, and Y. Zhang, J. High Energy Phys. 05 (2010) 048.

[18] W. Buchmuller, A. Ibarra, T. Shindou, F. Takayama, and D. Tran, J. Cosmol. Astropart. Phys. 09 (2009) 021; G. Kane, R. Lu, and S. Watson, Phys. Lett. B **681**, 151 (2009); P. Meade, M. Papucci, A. Strumia, and T. Volansky, Nucl. Phys. **B831**, 178 (2010); G. Hutsi, A. Hektor, and M. Raidal, J. Cosmol. Astropart. Phys. 07 (2010) 008; M. Cirelli and J. M. Cline, Phys. Rev. D **82**, 023503 (2010); N. Bernal and S. Palomares-Ruiz, arXiv:1006.0477; A. Cuoco, A. Sellerholm, J. Conrad, and S. Hannestad, arXiv:1005.0843; K. N. Abazajian, P. Agrawal, Z. Chacko, and C. Kilic, arXiv:1002.3820.

[19] J. Hisano, M. Kawasaki, K. Kohri, and K. Nakayama, Phys. Rev. D **79**, 063514 (2009); **80**, 029907(E) (2009).

[20] See, e.g., P. Gondolo and J. Silk, Phys. Rev. Lett. **83**, 1719 (1999); D. Hooper and G. D. Kribs, Phys. Rev. D **67**, 055003 (2003); G. Bertone, E. Nezri, J. Orloff, and J. Silk, Phys. Rev. D **70**, 063503 (2004); I. Cholis, L. Goodenough, D. Hooper, M. Simet, and N. Weiner, Phys. Rev. D **80**, 123511 (2009); T. Flacke, A. Menon, D. Hooper, and K. Freese, arXiv:0908.0899; M. R. Buckley, K. Freese, D. Hooper, D. Spolyar, and H. Murayama, Phys. Rev. D **81**, 016006 (2010); V. Barger, J. Kumar, D. Marfatia, and E. M. Sessolo, Phys. Rev. D **81**, 115010 (2010).

[21] J. Kumar, J. G. Learned, and S. Smith, Phys. Rev. D **80**, 113002 (2009).

[22] J. Hisano, M. Kawasaki, K. Kohri, and K. Nakayama, Phys. Rev. D **79**, 043516 (2009); J. Hisano, K. Nakayama, and Masaki J. S. Yang, Phys. Lett. B **678**, 101 (2009).

[23] L. Covi, M. Grefe, A. Ibarra, and D. Tran, J. Cosmol. Astropart. Phys. 04 (2010) 017.

[24] L. Covi, M. Grefe, A. Ibarra, and D. Tran, J. Cosmol. Astropart. Phys. 01 (2009) 029.

[25] D. Spolyar, M. Buckley, K. Freese, D. Hooper, and H. Murayama, arXiv:0905.4764.

[26] J. Liu, P. F. Yin, and S. H. Zhu, Phys. Rev. D **79**, 063522 (2009).

[27] S. K. Mandal, M. R. Buckley, K. Freese, D. Spolyar, and H. Murayama, Phys. Rev. D **81**, 043508 (2010).

[28] C. Wiebusch (IceCube Collaboration), arXiv:0907.2263.

[29] D. Hubert (IceCube Collaboration), Nucl. Phys. B, Proc. Suppl. **173**, 87 (2007); R. Abbasi *et al.* (IceCube Collaboration), Nucl. Instrum. Methods Phys. Res., Sect. A **601**, 294 (2009); C. Rott (IceCube Collaboration), arXiv:0810.3698; J. Braun and D. Hubert (IceCube Collaboration), arXiv:0906.1615; U. F. Katz (KM3NeT Collaboration), Nucl. Instrum. Methods Phys. Res., Sect. A **602**, 40 (2009); R. Abbasi *et al.* (IceCube Collaboration), Phys. Rev. D **82**, 072003 (2010).

[30] G. Servant and Tim M. P. Tait, Nucl. Phys. **B650**, 391 (2003).

[31] A. E. Erkoca, M. H. Reno, and I. Sarcevic, Phys. Rev. D **80**, 043514 (2009).

[32] A. E. Erkoca, G. Gelmini, M. H. Reno, and I. Sarcevic, Phys. Rev. D **81**, 096007 (2010).

[33] J. F. Navarro, C. S. Frenk, and S. D. M. White, Astrophys. J. **462**, 563 (1996).

[34] As a review, see G. Jungman, M. Kamionkowski, and K. Griest, Phys. Rep. **267**, 195 (1996); J. L. Feng, arXiv:1003.0904; L. Bergstrom, AIP Conf. Proc. **1241**, 49 (2010).

[35] A. Sommerfeld, Ann. Phys. (Leipzig) **403**, 257 (1931); J. Hisano, S. Matsumoto, and M. M. Nojiri, Phys. Rev. Lett. **92**, 031303 (2004); J. M. Russell, S. M. West, D. Cumberbatch, and D. Hooper, J. High Energy Phys. 07 (2008) 058; N. Arkani-Hamed, D. P. Finkbeiner, T. R. Slatyer, and N. Weiner, Phys. Rev. D **79**, 015014 (2009); I. Cholis, G. Dobler, D. P. Finkbeiner, L. Goodenough, and N. Weiner, Phys. Rev. D **80**, 123518 (2009); J. M. Russell and S. M. West, Phys. Lett. B **676**, 133 (2009); S. M. Koushiappas and M. Kamionkowski, Phys. Rev. Lett. **103**, 121301 (2009); M. Kamionkowski, S. M. Koushiappas, and M. Kuhlen, Phys. Rev. D **81**, 043532 (2010); M. Lindner, A. Merle, and V. Niro, arXiv:1005.3116; D. Suematsu, T. Toma, and T. Yoshida, Phys. Rev. D **82**, 013012 (2010); S. Hannestad and T. Tram, arXiv:1008.1511; J. L. Feng, M. Kaplinghat, and H.-B. Yu, Phys. Rev. D **82**, 083525 (2010); C. Arina, F.-X. Josse-Michaux, and N. Sahu, Phys. Lett. B **691**, 219 (2010).

[36] J. F. Beacom, N. F. Bell, and G. D. Mack, Phys. Rev. Lett. **99**, 231301 (2007); H. Yuksel, S. Horiuchi, J. F. Beacom, and S. Ando, Phys. Rev. D **76**, 123506 (2007); C. Delaunay, P. J. Fox, and G. Perez, J. High Energy Phys. 05 (2009) 099.

[37] T. K. Gaisser and M. Honda, Annu. Rev. Nucl. Part. Sci. **52**, 153 (2002); M. Honda, T. Kajita, K. Kasahara, S. Midorikawa, and T. Sanuki, Phys. Rev. D **75**, 043006 (2007).

[38] R. Enberg, M. H. Reno, and I. Sarcevic, Phys. Rev. D **78**, 043005 (2008).

[39] R. Abbasi *et al.*, Astropart. Phys. **34**, 48 (2010).

[40] E. Resconi (IceCube Collaboration), Nucl. Instrum. Methods Phys. Res., Sect. A **602**, 7 (2009).

[41] E. Middell, J. McCartin, M. D'Agostino (IceCube Collaboration), Proceedings of the 31st ICRC 2009.
[42] A. Strumia and F. Vissani, arXiv:0606054.
[43] S. I. Dutta, M. H. Reno, and I. Sarcevic, Phys. Rev. D **62**, 123001 (2000).
[44] A. B. McDonald, C. Spiering, S. Schonert, E. T. Kearns, and T. Kajita, Rev. Sci. Instrum. **75**, 293 (2004).
[45] P. Salucci, F. Nesti, G. Gentile, and C. F. Martins, arXiv:1003.3101, and references therein.
[46] G. Jungman and M. Kamionkowski, Phys. Rev. D **51**, 328 (1995).
[47] P. Lipari, Astropart. Phys. **1**, 195 (1993).
[48] G. Moreau and M. Chemtob, Phys. Rev. D **65**, 024033 (2001).